Species interactions, stability, and resilience of the gut microbiota - helminth assemblage in horses

Michel Boisseau, Sophie Dhorne-Pollet, David Bars-Cortina, Élise Courtot, Delphine Serreau, Gwenolah Annonay, Jérôme Lluch, Amandine Gesbert, Fabrice Reigner, Guillaume Sallé, et al.

Species interactions, stability, and resilience of the gut microbiota - helminth assemblage in horses

Michel Boisseau, Sophie Dhorne-Pollet, David Bars-Cortina, Élise Courtot, Delphine Serreau, Gwenolah Annonay, Jérôme Lluch, Amandine Gesbert, Fabrice Reigner, Guillaume Sallé, et al.

Species interactions, stability, and resilience of the gut microbiota - helminth assemblage in horses

Michel Boisseau
Université de Tours, INRAE, UMR1282 Infectiologie et Santé Publique
Sophie Dhorne-Pollet
Université Paris-Saclay, INRAE, AgroParisTech, GABI
David Bars-Cortina
Université Paris-Saclay, INRAE, AgroParisTech, GABI
Élise Courtot
Université de Tours, INRAE, UMR1282 Infectiologie et Santé Publique
Delphine Serreau
Université de Tours, INRAE, UMR1282 Infectiologie et Santé Publique
Gwenolah Annonay
INRAE, US UMR 1426, Genomic platform, 31326 Castanet-Tolosan, France
Jérôme Lluch
INRAE, US UMR 1426, Genomic platform, 31326 Castanet-Tolosan, France
Amandine Gesbert
INRAE, UE Physiologie Animale de l'Orfrasière, 37380 Nouzilly, France
Fabrice Reigner
INRAE, UE Physiologie Animale de l'Orfrasière, 37380 Nouzilly, France
Guillaume Sallé
Université de Tours, INRAE, UMR1282 Infectiologie et Santé Publique
Núria Mach (nuria.mach@inrae.fr)
IHAP, Université de Toulouse, INRAE, ENVT

Research Article

Keywords: anthelmintic, cyathostomin, nemabiome, nematode, metabarcoding, pyrantel, strongyle, 16S, ITS-2, RNAseq, immune response, IgA

Posted Date: August 16th, 2022

DOI: https://doi.org/10.21203/rs.3.rs-1955749/v1

Abstract

The nature and strength of interactions entertained among helminths and their host gut microbiota remain largely unexplored. Using 40 naturally infected Welsh ponies, we tracked the gut microbiota-cyathostomin temporal dynamics during parasite community removal and reassembly, and the associated host immune response. Infected ponies harboured 14 species of cyathostomins, overwhelmed by the abundance of Cylicocyclus nassatus. Parasite carriers exhibited gut environment modifications, higher Shannon entropy and orderly rearrangements of prokaryotic assemblages, with protective Clostridia species contributing to the successional nemabiome-microbiota crosstalk. Yet, the gut ecosystem was remarkably stable, and the host systemic response defined enrichment for B-cell activation and IgA production without corresponding changes in parasite burdens. Therefore, Clostridia microbial protection likely reduced fluctuating dynamics between the microbiota-parasite-host triad and favoured parasite tolerance. The system stability was disrupted by pyrantel treatment and parasite removal, with dire early consequences on the gut environment, microbiota diversity, and cytokine networks while highlighting the detrimental effect of cyathostomin burdens on Enterococcus spp. Both ecological communities were highly resilient to disturbance and recovered their pre-treatment compositions but for Cylicostephanus longibursatus in the parasite community. However, gut microbiotas failed to restore their original stability and shifted towards an interacting unstable state, with transient coexistence between Clostridia and core bacterial taxa, e.g. Fibrobacter and Prevotella, evoking their crucial role as stabilising forces for this new equilibrium. These observations highlight how anthelmintic treatment alters the gut microbiota stability and open new perspectives for adding nutritional intervention to current parasite management strategies in the field.

Introduction

Gastro-intestinal parasites and their host gut microbiota form a complex ecological system [1] harbouring direct [2, 3] and indirect interactions mediated through the modulation of the host immune system [4, 5]. Observations to date have shown diverse degrees of gut microbiota perturbations to helminth infection in humans [6–8], wild animal populations [9–13], species of veterinary interest like pigs [14, 15], ruminants [16–18], horses [19–23], and laboratory animals [3, 24–28]. Across studies, gastro-intestinal parasites are generally responsible for mild effects on the bacterial composition with little evidence of dysbiosis, although drastic modifications occur during clinical disease [21].

Still, these patterns of microbial shifts do not reflect the full range of dynamics needed to understand the contribution of microorganisms to host health [29–31]. Indeed, the stability of the gut microbiota also depends on the qualitative nature of the interactions between species [32]. In this respect, stability is thought to rely on competition between species and weak interactions between its parts [32, 33], while cooperation is destabilising [34].

To date, the characterisation of the interactions between species in helminth-infected hosts remains scant. Evidence for direct interactions between helminth and gut microbial species mainly bear on the

reciprocal feedback between *Lactobacillaceae* and *Heligmosomoides polygyrus* [3] or *Trichuris muris* in mice [35], or the need for gut microbiota attachment to *Trichuris muris* egg caps for triggering worm hatching [2].

Longitudinal monitoring of the helminth-gut microbiota system combined with methodological developments to account for non-linear trajectories [36] offers a powerful design to establish how a taxon responds to another, thereby isolating direct species interactions [5, 31]. Nevertheless, longitudinal observations of gut microbiota x helminth interactions are scarce (gathered from experimentally infected mice [37, 38], zebrafish [39] and sheep [16] or naturally infected horses [19, 20]) and often driven by investigating the consequences of parasite infection.

In addition to longitudinal observations, system disturbance [40], *e.g.* following drug treatment targeting the host microbiota or the parasite [5], offers a complementary strategy to unravel species interactions. This has been key to highlighting interactions between helminth and protozoan parasite species [11, 41] or investigating helminth community assembly in the wild [42]. Past experiments using this approach found little effect of *Trichuris* removal in infected mice [38] or humans [6]. Other experiments found that mebendazole treatment in pinworm-infected (*Enterobius vermicularis*) humans increased *Bifidobacterium longum* and *Oscillospira* spp and decreased *Faecalibacterium prausnitzii* and *Ruminococcus flavefaciens* [43]. After treatment, significant changes have also been reported in the gut microbiota of infected horses [22, 23].

Altogether, the nature of the interactions between the gut microbiota and helminth species remains largely unresolved. Understanding the source and consequences of dynamic variation in the host-parasite-microbiota ecosystem and how this complex system's stability is maintained is of particular interest to guide and evolve control strategies in the medical and veterinary settings. Here, we aimed to bridge this knowledge gap with longitudinal monitoring of the equine gut microbiota and parasite communities after parasite removal and reappearance.

Naturally infected horses lay an ideal setting for studying interactions between cyathostomin (small strongyles) species, their gut microbiota and the host systemic immune response. First, it represents a field situation which is not necessarily well characterised by artificial infection. Second, it allows longitudinal monitoring of the same individuals maintained under controlled conditions instead of wild surveys. Last, the cyathostomins - a complex of more than 50 species with worldwide distribution in grazing horses [44–46] - are in close contact with their host hindgut microbiome [47–49] that spans close to 5 000 genera from 95 phyla [49]. Using 40 naturally infected Welsh ponies maintained under controlled facilities during a 42-day trial, we explored the ecological resilience of both communities to parasite removal and re-appearance. Contrasting records from before and after anthelmintic treatment, we quantified compositional and interaction strength variations in the gut microbiota and nemabiome community while accounting for the host response using whole blood transcriptomic data. The results suggest strong resilience in both communities despite interaction strengths between bacterial genera

being affected by pyrantel treatment and support for inter-kingdom interactions between Clostridia, core taxa and cyathostomins

Results

A group of ten naturally infected female ponies (high shedders treated, HIGH_TRT) were given pyrantel treatment to remove adult cyathostomin while leaving developing stages to resume their development over a 42 day-trial (Fig S1; Table S1). Metabarcoding data of the gut microbiota and cyathostomin species were produced to quantify inter-species interactions and resilience in both communities. They were matched with control groups, being either high shedders untreated (HIGH_CTL; positive control) and low shedders treated (LOW_TRT; intrinsic pyrantel effect) or left untreated (LOW_CTL; negative control). Within each group, a subset of six ponies had their whole blood transcriptomic profiles determined as a control for the host response to the system.

Global overview of the host - cyathostomin - gut microbiota system

Following prokaryotic data processing ($\sim 1.6 \cdot 10^8$ 16S rRNA sequences; 30 793 ± 6 391.3 sequences per sample), 7 545 Amplicon Sequence Variants (ASV) were identified, out of which 69.02% were assigned down to the genus level (Supplementary information). They encompassed 11 phyla, 87 families, and 179 genera matching previous studies in European horses [50–52] (Table S2). Firmicutes (46.8 ± 0.39%) dominated the assemblage, followed by Bacteroidetes (31.5 ± 0.42%), Fibrobacteres (10.5 ± 0.48%), and Spirochaetes (8.40 ± 0.22%; Fig S2a). At the genus level, 12 genera defined a cross-sectional and -temporal core (Fig S2b). *Fibrobacter* (15.07 ± 0.6%), unclassified *Lachnospiraceae* (12.22 ± 0.26%), and *Treponema* (12.07 ± 0.29%) accounted for one-third of the total abundance (Fig. 1a).

The initial cyathostomin community comprised 239 ASVs (Table S3), spanning 14 species and three genera (Fig. 1b). Species prevalence was high, with eight species found in more than 17 out of 19 high shedders. *Cylicocyclus leptostomum* and *Coronocyclus labiatus* were found in 14 out of 19 ponies. On the contrary, relative abundance was overdispersed and dominated by *Cylicocyclus nassatus* (52.6%; the only species found in every sample at day 0 and day 42), *Cylicostephanus minutus* (22.2%) and *Cylicostephanus calicatus* (10.1%; Table S4).

The HIGH_CTL individuals experienced neither weight loss nor gastrointestinal disorders compared to their uninfected counterparts. Their average FEC was 867 eggs/g, *i.e.*, 8- to 21-fold higher (adj $P = 9.11\ e^{-18}$) compared to LOW_CTL ponies at any time (FEC = 69 eggs/g). They also exhibited higher concentrations of faecal DNA (Fig. 1c; adj $P = 9.48\ e^{-07}$), suggestive of higher microbial and parasite (eggs) biomass and host-derived contents from epithelial cells and blood-shedding into the lumen. This was concomitant to increased faecal pH (adj $P = 0.00016$; Fig. 1d).

Figure 1: Global overview of the host - cyathostomin - gut microbiota system

(a) Taxonomic bar plots of the top 20 dominant genera in the gut microbiota according to the experimental groups. Colours denote microbial genera. Taxonomic inference relied on the QIIME closed-reference approach against the SILVA database at a sequence similarity level of 99%; (b) Relative abundances measured in the cyathostomin community in high shedders using ITS-2 barcodes; (c-d) Violin plots showing the concentration of faecal DNA and pH in faeces, respectively, according to the HIGH and LOW control groups. Boxplots show the median, 25th, and 75th percentile, the whiskers indicate the minima and maxima, and the points lying outside the whiskers of box plots represent the outliers. Adjusted p values from two-sided Wilcoxon rank-sum test

On day 0, parasite infection left a marked transcriptomic signature in the whole host blood with 1 203 differentially expressed genes (610 up-regulated and 593 down-regulated; Supplementary information and Table S5), encoding functions related to IL7, NF-kappa B signalling, and B cell activation (Supplementary information). In line with this, the infection status accounted for 5.5% of the gene variance on average overall (Supplementary information). The 117 genes with stronger statistical support (π score above 2) defined significant enrichment for B-cell activation (GO:00421113, adj $P = 0.002$), and KEGG intestinal immune network for IgA production (KEGG:04672, adj $P = 0.004457338$) among others (Supplementary information; Table S6).

Cyathostomin infection hence significantly modifies the physical environment in which they live and the host immune response.

Helminth infection defines a stable assemblage with higher microbial diversity and species turnover in infected ponies

We next investigated how the infection status affected the interactions between the bacterial and cyathostomin communities. Overall, the infected ponies harboured gut microbiotas distinct from the non-infected subjects (PerMANOVA; $R^2 = 0.07823$, $P = 0.001$; Fig. 2a). Differences were confirmed via analysis of similarity (ANOSIM; R = 0.1023, $P = 0.001$). When β-diversity was analysed separately for each infection status, the turnover was higher in the ponies excreting more parasite eggs (two-sided Wilcoxon rank-sum test, $P = 2.2\ e^{-16}$; $\beta_{TURN} = 0.669 \pm 0.0876$ and $\beta_{TURN} = 0.661 \pm 0.0794$, respectively). This was concomitant with increased nestedness (two-sided Wilcoxon rank-sum test, $P = 5.99\ e^{-52}$, $\beta_{NEST} = 0.036 \pm 0.0464$ and $\beta_{NEST} = 0.031 \pm 0.0398$, in high and low shedders, respectively) and Shannon entropy (GLM, $P < 0.01$; Fig. 2b) in that group, suggesting that parasites in the lumen increase the diversity of assemblages and gain of invasive or rare species.

Despite the significant turnover found in the presence of patent cyathostomin infection, the dynamic stability of the bacterial assemblage remained below one (the instability threshold) in untreated ponies over the considered 42 days (Fig. 2c). The dominance of relatively weak interactions and the Simpson's diversity index provided further empirical support for the system's stability and high coexistence during infection (Fig. 2d-e). Stability also matched the increase in FEC (Fig. 2f) underscoring the stabilising effect of parasite infection. Additionally, the successional β-diversity dispersions were homogeneous

across high- and low-shedder groups (distance to centroid = 0.162 ± 0.0038; adjusted $P = 0.5341$; Fig. 2g). Therefore, faecal microbial communities differed from baseline after a day as after one week or one month.

In accordance with the high turnover, the ecological patterns largely varied within infected individuals, suggestive of constant re-arrangements in the inter-genera interaction strengths (Fig. 2d). We show substantial temporal variation for a set of 51 genera in control individuals (Table S7), including core bacteria and many rare Clostridia. For 84% of these genera, day-to-day abundance variation was substantially larger within than between high-shedders (intraclass correlation coefficient (ICC) [53] < 0.5; Table S8; Fig. 2h). Within a few weeks, significant extensive changes in abundance (~ 100-fold changes) occurred for 13% of the genera (Table S8). On the contrary, core genera were generally more stable (*e.g. Prevotella* ($ICC_{within} = 0.649$) and *Ruminococcus* ($ICC_{within} = 0.653$)), evoking possible stabilising factors of the core microbiota under parasite infection.

Figure 2: Helminth infection defines a stable assemblage despite the higher microbial richness and species turnover in infected ponies

(a) NMDS ordination analysis (Bray Curtis distance) of the ASV composition. Points denote individual samples which are coloured according to the experimental group: HIGH_CTL (violet), HIGH_TRT (red), LOW_CTL (cyan), and LOW_TRT (blue). The shape of the dots indicates the level of parasitism: round (HIGH) and triangle (LOW); (b) Longitudinal evolution of Shannon diversity across time for high and low shedding individuals. Shaded areas represent 95% confidence intervals; (c-f) Time-varying stability, interaction strength, Simpson's diversity index and FEC value for the microbial communities in each group using the Multispatial convergent cross-mapping; (g) Bray Curtis distance to the centroid of the gut microbial ASVs between the HIGH and LOW control groups. Boxes show median and interquartile range, and whiskers indicate 5th to 95th percentile; (h) Within-subject variance based on the interclass correlation coefficient (ICC) as part of the total variance in genus abundance for all genera significantly affected between high and low shedders across time; (i) Multispatial convergent cross-mapping (CCM) results showing causal relationships between FEC and the abundances of different taxa. Solid lines indicate cross-map skill (ρ) from dynamic stability to another variable, which represents the causal influence of that variable on dynamic stability. Shaded regions indicate 95% confidence intervals of 1 000 surrogate time series. Cross-map skills (ρ) reported here were all significant

Out of the 51 genera studied here, 54.90% of the genera ($n = 28$) exhibited significant causal interactions with one another ($P \leq 0.05$). For instance, Clostridia species were jointly determined and mutually influenced by core species (all $P \leq 0.05$), namely *Fibrobacter, Saccharofermentans*, and *Prevotella* (Table S9). In agreement with this notion, there was a direct causal relation between FEC and the abundance of less abundant Clostridia taxa, namely *Lachnoclostridium* ($P = 0.07$), *Terrisporobacter* ($P = 0.028$), and *Ruminococcaceae* ($P = 0.037$; Fig. 2i, Table 1). This association between Clostridia taxa and parasite infection was conserved in the validation set (Supplementary information).

Moreover, the CCM analysis showed significant interactions between phylogenetically distant bacterial genera and cyathostomin species, whereby bacteria forced cyathostomin successional trajectories (Table 1; Fig S3). The dependence of nemabiome on microbiota encompassed four cyathostomin taxa (Table 1). Precisely, the abundance of the rare *C. leptostomum* was driven by stable acetogens. The opposite occurs in the case of *Cyathostomum pateratum*, which forced *Vallitalea* abundances (P = 0.034), suggesting that this taxon actively depends on parasite presence or/and activity to improve its survival.

Table 1
Significant causal interactions between gut bacteria and cyathostomin species or the faecal environment

Interactant a	Interactant b	Treatment	*P*-value *(a forces b)*	*P*-value *(b forces a)*
Cylicocyclus nassatus	*Papillibacter*	TRT	0.042	0.811
Cylicostephanus minutus	*Anaerotignum*	TRT	0.031	0.647
Cylicostephanus sp	*Bacteroides*	TRT	0.046	0.317
Coronocyclus labiatus	*Corynebacterium*	CTL	0.42	0.031
Cyathostomum catinatum	*Frisingicoccus*	CTL	0.507	0.011
Cyathostomum pateratum	*Vallitalea*	CTL	0.034	0.499
Cylicocyclus leptostomus	*Acetitomaculum*	CTL	0.731	0.049
Cylicocyclus leptostomus	*Alloprevotella*	CTL	0.242	0.017
Cylicocyclus leptostomus	*Escherichia/Shigella*	CTL	0.504	0.047
Cylicocyclus leptostomus	*Marvinbryantia*	CTL	0.684	0.033
Cylicocyclus leptostomus	*Christensenellaceae**	CTL	0.715	0.033
Cylicostephanus minutus	*Alloprevotella*	CTL	0.492	0.014
Cylicostephanus minutus	*Corynebacterium*	CTL	0.648	0.046
Cylicostephanus sp	*Parapedobacter*	CTL	0.624	0.037
pH	*Lachnoclostridium*	TRT	0.442	0.036
DNA	*Christensenellaceae**	TRT	0.016	0.669
FEC	*Labilibacter*	CTL	0.023	0.012
FEC	*Lachnoclostridium*	CTL	0.007	0.519
FEC	*Terrisporobacter*	CTL	0.028	0.016
FEC	*Ruminococcaceae.1**	CTL	0.037	0.516
FEC	*Weissella*	CTL	0.023	0.924
DNA	*Parapedobacter*	CTL	0.877	0.015

* unclassified genera

Altogether, infected subjects harbour a richer, more dynamic community. Still, the ecosystem was drawn to stability and a resistant configuration underpinned by protective Clostridia taxa shaping the

nemabiome-microbiota ecosystem dynamics.

Parasite removal has a drastic and acute effect on the gut environment and microbiota composition, but limited response in the host blood

We first determined if pyrantel administration provided a favourable gut environment for the expansion of certain bacterial species or induced changes in the host immune response. The treatment induced a 5% drop in faecal pH measured in the LOW_TRT ponies (GLM, all $P < 0.05$). This reduction in faecal pH explained 20.2 and 17.3% of the variance in the host expression levels of neuroligin (*NLGN2*) and a solute carrier (*SLC10A7*) coding genes (Fig S4). Transcript counts of both genes were reduced at day 1 in the treated ponies ($\beta_{HIGH\_TRT \times day\ 1} = -5.66$, $P = 0.06$ and $\beta_{HIGH\_TRT \times day\ 1} = -73$, $P = 0.01$, for *NLGN2* and *SLC10A7*, respectively), compatible with a direct effect of the pyrantel treatment on the host. Otherwise, the pyrantel treatment contributed little to the variance in host gene expression (2.92% on average, Supplementary information, Fig S5) with no evidence of an inflammatory response, as previous data suggested [54].

In the HIGH_TRT ponies, pyrantel treatment decreased faecal egg count by 87.5% (95% c. i. ranging from 78.5–93.7%), with a significant egg reappearance period reached by day 35.

Parasite removal in the high shedders furthered the sharpest reduction in faecal pH 24h post-treatment (pH difference = -0.28; $P = 0.0538$, Fig. 3a). This was coupled with acute disbalance of the gut microbiota β-diversity in HIGH-TRT individuals and significant changes from the original state from 18 to 24 h post-treatment, when the host expelled the worms (Dunn test of mean Bray Curtis distance within time points, adj $P = 3.14\ e^{-05}$; Fig. 3b). Accordingly, a skewed decrease in nestedness ($\beta_{NEST} = 0.027 \pm 0.03$; GLM; $P = 0.00154$) and microbial richness (GLM; $P = 0.0012$) was observed at 18h post-treatment.

Parasite removal had slight but noticeable effects on the host blood transcriptomic response. In high-shedders, the treatment and treatment x time interaction respectively explained 1.42% and 1.47% of gene expression variance on average (Fig S5; Supplementary information). A comparison between the treated and untreated ponies 24h post-treatment found 13 differentially expressed (DE) genes (Table 2).

Table 2. Genes differentially expressed between the treated and untreated ponies 24h after pyrantel administration

For each gene, the log-transformed fold change with associated standard error (in brackets) and adjusted *p*-value (Benjamini-Hochberg correction) are given.

Gene name	Description	Log(Fold-change) (s.e.)	Adj *P*-value
UBASH3B	ubiquitin associated and SH3 domain containing B	-22.29 (3.01)	1.87E-09
CCL8	chemokine (C-C motif) ligand 8	2.33 (0.35)	1.56E-07
ENSECAG00000020341	N/A	0.68 (0.15)	1.32E-02
IFI44	interferon induced protein 44	1.15 (0.26)	2.04E-02
SWSAP1	SWIM-type zinc finger 7 associated protein 1	0.8 (0.18)	2.04E-02
NINJ1	ninjurin 1	1.17 (0.26)	2.04E-02
ENSECAG00000032959	N/A	-0.98 (0.22)	2.04E-02
ENSECAG00000037799	N/A	2.51 (0.56)	2.04E-02
H2BC21	H2B clustered histone 21	1.3 (0.3)	2.54E-02
KLK15	kallikrein related peptidase 15	-1.61 (0.38)	2.92E-02
TLR5	toll like receptor 5	0.64 (0.15)	3.45E-02
TRIM35	tripartite motif containing 35	0.52 (0.13)	4.87E-02
ILT11A	immunoglobulin-like transcript 11 A	0.54 (0.13)	4.99E-02

In addition, the top 5% of genes most affected by treatment in high-shedders defined significant enrichment for interferon-related pathways, IL-27 signalling pathways, and nucleotide-binding oligomerisation domain (NOD) ligand-associated signalling, resulting in highly selective recognition and reactivity pattern in response to invasion (Supplementary information).

Figure 3: Parasite removal has a drastic effect on the gut environment and microbiota composition, but limited response in the host blood

(a) Evolution of faecal pH across time in high shedders. To display differences between group series, the ribbon was filled with red colour when the max in HIGH-CTL was higher than the min in HIGH-TRT, and in cyan colour when the maximum in HIGH-TRT was higher than the min in HIGH-CTL; (b) Dendrogram plot

based on the within-time and between time dissimilarities in the HIGH-TRT group. The leaf segment is reversed if some time points are more heterogeneous than the combined time class. The horizontal line is drawn at the level of mean between-time dissimilarity, and vertical lines connect within-time dissimilarities to this line; (c) NMDS ordination analysis (Bray-Curtis distance) of the ASV composition in HIGH_CTL (violet), and HIGH_TRT (red) samples across the time points; (d) *Enterococcus* count distribution in the untreated (CTL) and treated (TRT) low- and high-shedders. Boxplots are coloured according to whether counts were measured before (grey or blue) or after (red or yellow) significant parasite reappearance period (28 days after pyrantel treatment); (e) Trajectory of *Enterococcus* and *Cyathostomum pateratum* in the infected untreated and treated ponies

Altogether, these observations suggest that pyrantel treatment *per se* had little effect on the gut microbiota or the host response, but parasite removal was a major disturbance to the gut ecosystem with slight but noticeable changes in the host blood transcriptome.

Both the parasite and gut microbiota communities displayed strong resilience after treatment

Following treatment, the gut microbiota composition rebounded to baseline level 48h after pyrantel treatment (Fig. 3c). As specific examples, *Treponema, Cellulosilyticum*, and *Eubacterium ruminantium* genera sharply decreased by day 1 but recovered by day 3, showing a solid resilience along the timeline (MaAsLin, adj $P = 0.04584$; Table S10).

On the parasite side, the first available nemabiome data were produced for two individuals at 28- and 35-days post-treatment. On both occasions, *C. nassatus*, *C. minutus* and *Coronocyclus coronatus* represented more than 95% of total abundance, although a more diverse combination (*C. nassatus*, 68.9%; *C. longibursatus*, 8.3%; *C. minutus*, 6.5%; *C. coronatus*, 3.8%, and *C. pateratum*, 3.2%) was found in one pony at day 35. After 42 days, pyrantel treatment reduced cyathostomin Simpson's index (Wilcoxon's test = 30, $P = 0.048$) but not Shannon's index (Wilcoxon's test = 29, $P = 0.07$), suggestive of an effect bearing on the most dominant taxa. In line with this, differential species count modelling found a significant reduction in *C. longibursatus* abundance (4th most abundant species) upon treatment (Wald test = -3.01, adj. $P = 0.038$). This latter observation underscored the cyathostomin community resilience to the treatment (despite short-term pyrantel efficacy), as suggested by its non-significant effects on the β-diversity ($F_{1,20} = 2.92$, adj. $P = 0.11$, $R^2 = 0.21$ for Jaccard distance; $F_{1,20} = 1.64$, adj $P = 0.43$ and $R^2 = 0.07$ for Bray Curtis dissimilarity).

We then sought bacterial members most affected by parasite re-emergence. Abundance of *Enterococcus* spp - represented by members of the *E. asini* (54.37%), *E. mediterraneensis* (38.23%) and *E. casseliflavus* (7.36%) - was lower in the high-shedders before treatment (Fig. 3d); $\beta_{HIGH} = -0.99 \pm 0.3$, $P = 0.001$; MaAsLin, adj $P = 0.0458$; AUROC = 0. 6230 and recall of 73.84%). Following worm re-emergence, this rare genus was significantly disfavoured in the treated high-shedders ($\beta_{After\ treatment\ x\ Treated\ x\ HIGH} = -2.62 \pm$

0.69, $P = 9.80\ e^{-06}$; Fig. 3d). Inspection of pairwise relationships with CCM found evidence of *C. pateratum* directly forcing this genus in the treated ponies ($P = 0.07$; Fig. 3e).

Pyrantel treatment and parasite removal pushed the gut microbiota towards an alternative state

Following pyrantel treatment, the microbiota composition remained unchanged in the low shedders (PerMANOVA; $R^2 = 0.0169$, $P = 0.793$), with a similar degree of heterogeneity across time (lme; $P = 0.3353$), and no shifts in individual taxa including those endowed with the capacity of utilising nutrients more available in inflamed tissue (MaAsLin, adj $P > 0.5$). Conversely, variation in Shannon index (GLM; $P = 5.43\ e^{-06}$), core dominance (GLM; $P = 5.12\ e^{-08}$) and rarity (GLM; $P = 6.11\ e^{-09}$) coefficients suggested ecosystem destabilisation (Fig S6a-c).

The microbiota dynamic stability following pyrantel treatment and parasite removal was significantly shifted towards less stable states in the high shedders on day 7 (β_{HIGH_TRT} between 0.19 ± 0.09, $P = 0.038$; Fig. 2c) and to a lesser extent on day 15 ($\beta_{HIGH\_TRT} = 0.16 \pm 0.09$, $P = 0.08$; Fig. 2c). In addition, the dominance of weak interactions between bacterial species was mildly driving dynamic stability in the treated ponies ($P = 0.08$; Fig. 2d), whereas Simpson's diversity was the main driving force of this stability in the lack of treatment ($P = 0.07$; Fig. 2e). This recalls that cyathostomin infection increases gut microbiota complexity, and would be compatible with decreasing weak interactions following parasite removal. In line with a putative stabilising effect of the cyathostomin presence on the gut microbiota, increasing FEC matched more stable states (Spearman's $\rho = -0.28$, $P < 10^{-4}$; Fig. 2f).

While the increased instability matched the reduction in FEC, there was no statistical support for concomitant variation in other community diversity indices or interaction strengths. Interaction strength (S-map coefficients) inspection highlighted significant changes in the relationship between a few species' pairs. More than half of the 16 most disrupted trajectories involved interactions acting on the *Oscillospiraceae* (class Clostridia) or the pathobiont *Escherichia/Shigella* complex (Table S11).

Similarly, our causal models revealed additional Clostridia as causal drivers of the perturbed ecosystem, including *Blautia, Lachnoclostridium, Ruminoclostridium*, and unassigned *Oscillospiraceae, Christensenellaceae* and *Ruminococcaceae* taxa (Table 3).

Table 3
Significant causal interactions between gut bacteria following treatment perturbation

Interactant a	Interactant b	*P*-value *(a forces b)*	*P*-value *(b forces a)*
Fibrobacter	*Oscillospiraceae**	0.562	0.012
Prevotella	*Rikenellaceae**	0.634	0.012
Fibrobacter	*Rikenellaceae**	0.381	0.022
Papillibacter	*Ruminiclostridium*	0.151	0.023
Hungateiclostridium	*Oscillospiraceae**	0.489	0.024
Parapedobacter	*Vallitalea*	0.55	0.032
Bacteroides	*Prevotella*	0.486	0.034
Hungateiclostridium	*Labilibacter*	0.793	0.037
Eubacterium hallii group	*Treponema*	0.485	0.038
Blautia	*Marvinbryantia*	0.094	0.042
Lachnoclostridium	*Parapedobacter*	0.816	0.044
Hungateiclostridium	*Saccharofermentans*	0.769	0.046
Blautia	*Ruminococcaceae.1**	0.046	0.203
*Christensenellaceae**	*Ruminococcaceae.1**	0.014	0.255
*Rikenellaceae**	*Weissella*	0.029	0.329
Lachnoclostridium	*Defluviitaleaceae**	0.047	0.347
Escherichia/Shigella	*Weissella*	0.03	0.528
Corynebacterium	*Vallitalea*	0.027	0.665
Anaerotignum	*Parabacteroides*	0.047	0.729

* unclassified genera

We also find that core species considered functionally relevant in the gut exhibited tight interactions with Clostridia (*e.g. Saccharofermentans, Treponema, Prevotella*, and *Fibrobacter*, Fig. 4a), evoking the abundant and ubiquitous core taxa have major ecological roles in ensuring ecosystem stability despite environmental disturbances. This was also highlighted by the fact that core microbiota exhibited the greatest degree of connection (higher interactions number and strength) in response to treatment (Fig. 4bc). Last, the pathobiont *Escherichia/Shigella* was a casual driver of the lactic acid bacteria

Weissella [55] (ρ = 0.204; P = 0.03), confirming that external stimuli may foster blooms of otherwise low-abundance bacteria that may contribute to modify the gut environment.

Figure 4: Core taxa connection ensures ecosystem stability upon environmental perturbations

(a) Ecological association inference of core taxa using the S-map method. Microbial nodes are coloured by order. Taxa highlighted in bold represents the core clades. Edge width corresponds to the strength of the association between features (S-map coefficients); (b-c) Density plot of all interactions and their strength in response to treatment

We next investigated specific interactions between bacterial genera and the parasite community based on parasite reappearance. While bacteria generally forced parasite abundances in untreated ponies, the opposite was true in treated ponies. In this group, direct causal relations were found between *C. minutus* and *Anaerotignum* (P = 0.031), and *C. nassatus* and *unassigned Cylicostephanus* were significant drivers of *Papillibacter* (P = 0.042) and *Bacteroides* (P = 0.046; Table 1), respectively. Other cyathostomin x bacteria interactions found in the untreated ponies were no longer observed in their treated counterparts, compatible with direct antagonistic relationships between both populations (Table 1).

Therefore, pyrantel treatment and parasite removal induced shifts in the community interaction and physiological changes in the gut that affected the long-term stability of the microbiota for as long as six weeks after treatment.

Discussion

Interactions between helminth species and the gut microbiota have been extensively studied, but the extent of their resilience and long-term ecological stability after perturbation was yet unclear. Using a controlled horse-cyathostomin system with rapid and not invasive sampling (*e.g.* stool DNA and blood RNA sequencing), this study opens several strands of research for managing parasite infection in the field.

The cyathostomin infection affected the gut bacterial communities and the host immune response with a mild impact on the host's health. Of note, this complex ecosystem showed striking long-term stability, suggesting a well-adapted and balanced triad (host - microbiota - parasite) and the crucial role of Clostridia. First, Clostridia limited the overgrowth of pathobionts that might slow infection tolerance or support inflammatory [56]. Second, our observations combined with the validation cohorts [19, 20, 22, 57] confirmed that parasite infection was tightly linked to the class of Clostridia [24, 58]. Many of the observed Clostridia, namely *Blautia, Clostridium, Eubacterium, Ruminococcus*, and *Oscillibacter*, are known to convey health benefits and boost anti-inflammatory responses (*e.g.* regulatory T cell-induction [59, 60]) through SCFA production [61] or bile acid transformation [62]. It seems conceivable that, beyond their role in carbohydrate metabolism, Clostridia interspecific interactions contributed to setting the tone of immune tolerance in horses [63]. Supporting this notion, observations in *Caenorhabditis elegans* already established how the host gut microbiota could shape the evolutionary trajectory of its host

towards tolerance to pathogens and the resulting adaptive response of the pathogen to microbial agents [64]. Such reactions against a system as diverse as that found in horses [49] might, in turn, have had a significant role in the diversification of cyathostomin species.

The sharp disruption of this complex tripartite relationship had significant implications for all players in the ecosystem. On the one hand, anthelmintic treatment and parasite removal lead to substantial but reversible dire shifts in the gut microbiome composition and host immune response, including IL-27 activation and interferon-associated pathways. IL-27 is an epithelial-derived alarmin with chief functions in T-reg cell parasite immunity and maintenance of intestinal homeostasis [65]. On the other hand, the cyathostomin community also showed strong resilience following treatment but for *C. longibursatus*, mirroring independent results from wild buffalo [42]. This contradicts past observations from the Netherlands, where *C. longibursatus* dominated after pyrantel treatment [66] and may owe to a distinct drug resistance profile in our population. Because pyrantel targets the luminal stages and ponies were maintained under parasite-free conditions, cyathostomin re-assembled from the developing stages harboured in the intestinal mucosa. This undoubtedly contributed to limited variation in their structure 42 days post-treatment. In this respect, longitudinal monitoring of grazing individuals after a suppressive treatment like moxidectin - the drug with the current highest efficacy against developing and encysted larval stages [67] - would help sorting the contribution of putative priority effects between cyathostomin species and explore how the gut microbiota or environmental variables contribute to the community reassembly [42] along with the host response.

Although the overall microbiota displayed quick and robust resilience to disturbance, the interacting network remained less stable for as long as six weeks after treatment because of changes in interaction strength and population dynamics. As such, these observations expand past studies focused on the consequences of parasite infection [7, 12, 19, 20, 39] or anthelmintic treatment on the composition of the host gut microbiota [6, 23, 24, 38, 43, 68–71]. The ecosystem instability following anthelmintic treatment and parasite removal is compatible with the “Anna Karenina principle”, where uneasy communities vary more strongly than non-challenged communities [72], and environmental changes can more easily tip the balance, especially in aged hosts experiencing recurrent infections and regularly subjected to prophylactic anthelmintic treatments. Therefore, repeated rounds of anthelmintic administration may hamper the buffering of other undergoing stresses and increase the susceptibility to medical comorbidities due to the decreased complexity and stability of microbial community [73, 74] or to different indirect host pathways [40].

The interactions between a large swath of Clostridia and core taxa likely counteracted the consequences of drug administration. They appeared, therefore, as promising gatekeepers to promote healthy and stable microbiomes [75]. Increasing dietary fibre with derived polysaccharides needed to expand core taxa and Clostridia (*e.g.* fructans, inulin, xylans, and arabinoxylan) could be the front-line for nutritional interventions [76] in anthelmintic treatment programs. Additionally, the administration of strict anaerobes Clostridiales could grant rapid recovery of the ecosystem properties and holobiont fitness after acute insults like drug treatment. As such, our findings complement past observations on the impact of gut

microbiota on treatment outcomes in humans [77]. Combined with good management practices, strategic diet manipulation could be part of the helminths control program [29].

Additional data from bottom-up functional approaches and reductionist experiments [31] considering a few bacterial species of interest exposed to defined components (*e.g.* helminth larvae or eggs) should prove crucial in predicting the mechanisms responsible for helminth-microbiome interactions and better forecasting drug treatment effects. Such a system could also support the seemingly competitive relationship between *Enterococcus* spp and the cyathostomin community, among which *C. pateratum* is a likely disruptor. *Enterococcus* is a rare taxon not found in the validation cohort, preventing any validation of the association with cyathostomin infection. Nonetheless, monitoring changes in the abundance of this rare microbe, which appears to be more sensitive to parasite fluctuations and more prone to extinction, might serve as an early warning system of cyathostomin infection in horses.

Overall, this study highlighted the detrimental effect of cyathostomin infection on *Enterococcus* spp members but the protective role of Clostridia and core taxa (*e.g.* gatekeepers) to cascade the community stability and host immune tolerance towards cyathostomins. It also revealed a microbial community that bent with global rearrangements after pyrantel treatment yet exhibited resilience but shifted towards another interacting and unstable state through which the abundance of co-infecting parasite strains influenced the assemblage. A more comprehensive field study and deeper functional resolution of the host-gut microbiota-parasite system will be essential to anticipate how this drug-defined equilibrium may affect functional redundancy in the bacterial community and the assembly of the parasite community on pasture.

Materials And Methods

Ethical statement

The local animal care and use committee reviewed and approved the study protocol (CEEA Val de Loire; reference: APAFIS#17427-2018080211451233 v7). All protocols were conducted following EEC regulation (no 2010/63/UE) governing the care and use of laboratory animals, effective in France since the 1st of January 2013.

Animal cohort selection and maintenance

Forty female Welsh ponies (average age 4.77 ± 2.05 years) were selected from an experimental herd of 107 ponies [78] regularly monitored for FEC during the grazing season since 2013. The selection was based on the FEC records database consisting of 703 observations of the whole herd at the time of selection. Every individual pony had been recorded at least three times over a minimum of two years (seven observations per pony on average across the entire herd). FEC data were log-transformed to correct for overdispersion and fitted a linear mixed model accounting for environmental fixed effects (month of sampling, year of selection, time since last treatment, age at sampling) as previously described

[19, 79]. The individual was considered a random variable to account for the intrinsic pony susceptibility against cyathostomin infection. Based on these estimates, the 40 individuals with the most extreme forecast were chosen to create two groups of high- (HIGH) or low-shedders (LOW). The median FEC was 515.28 ± 564.04 for HIGH and 41.17 ± 99.99 for the LOW groups across the past six years.

The 40 Welsh ponies grazed from mid-April to the first week of October 2019 in a group across 19 hectares. During that time, they were subjected to targeted pyrantel treatment (Strongid® oral paste, Zoetis, Paris, France, 1.36 mg pyrantel base per kg of body weight) based on FEC measurements in mid-July 2019. They had a variable anthelmintic history but received no larvicidal treatment directed at immature cyathostomins stages three months before the study. Neither had antibiotic or anti-inflammatory therapy in the previous two months (Fig S7). Intestinal disorders such as colic were recorded in one individual before the start of the study. The horse was treated with the antipyretic metamizole (Dipyralgine®, Med'Vet, France, 5 mL per 100 kg of body weight) but did not receive antibiotics (Fig S7).

In September 2019, all individuals were housed and maintained in groups of three under natural light conditions in a 14 m^2 pen with slatted floors, which precluded further nematode infections. Animals were fed 5 kg of hay per day and 600 g of concentrate pellets (Tellus Thivat Nutrition Animale Propriétaire, Saint Germain de Salles, France) consisting of barley (150 g/kg), oat bran (162 g/kg), wheat straw (184.7 g/kg), oats (200 g/kg), alfalfa (121.7 g/kg), sugar beet pulp (50 g/kg), molasses (30 g/kg), salt (7.3 g/kg), carbonate Ca (5.5 g/kg), and a mineral and vitamin mix (2 g/kg), on an as-fed basis. The mineral and vitamin mix contained Ca (28.5%), P (1.6%), Na (5.6%), vitamin A (500,000 IU), vitamin D3 (125,000 IU), vitamin E (1,500 IU), cobalt carbonate (42 mg/kg), cupric sulfate (500 mg/kg), calcium iodate (10 mg/kg), iron sulfate (1 g/kg), manganese sulfate (5.8 g/kg), sodium selenite (16 mg/kg), and zinc sulfate (7.5 g/kg) on an as-fed basis. In all cases, the concentrate in the stalls was offered and controlled individually by a caretaker who monitored the animals daily to ensure they were not sick or injured. Water was available *ad libitum.* The study provided no food additives, prebiotics, or probiotics that could affect gut microbiota composition. The study described herein started after a 3-week acclimation period that was considered sufficient to account for changes in diet composition, management, and environmental conditions.

Study design and sampling

On day 0, the HIGH and LOW groups were randomly divided into two subgroups blocked for age. The subgroups HIGH-TRT and LOW-TRT received a dose of pyrantel (Strongid® oral paste, Zoetis, Paris, France, 1.36 mg pyrantel base per kg of body weight) to eliminate the adult worms in the gut lumen while leaving developing stages untouched. Subgroups HIGH-CTL and LOW-CTL were not treated. To monitor the immediate anthelmintic treatment effect on gut microbiota, faecal material was collected 15, 18, 21, 24, 48, and 72 hours after treatment, corresponding to faecal excretion of the drug [80]. Then, every pony was subjected to longitudinal monitoring of faecal strongyle egg excretion and faecal microbiota weekly,

including days 7, 15, 21, 28, 35, and 42 post-treatment (Fig S1). This established interaction patterns within the bacterial community and between the parasite and bacterial communities. On day 0, samples were collected before the anthelmintic treatment. The body weight of the animals was recorded every fifteen days.

Faecal sampling, faecal pH measurement, and coprology

Fresh faecal samples were collected from the rectum at every time point. Faecal aliquots for microbiota analysis were immediately snap-frozen in liquid nitrogen and stored at −80°C until DNA extraction. In contrast, faecal aliquots were processed on-site to measure the cyathostomin eggs' faecal excretion level, and initiate larval culture for community composition analysis. The pH in the faeces was determined after 10% faecal suspension (wt /vol) in saline solution (0.15 M/ml NaCl solution).

FECs were measured as a proxy for patent cyathostomin infection. FEC was carried out using a modified McMaster technique [81] on 5 g of faeces diluted in 70 mL of NaCl solution with a density of 1.2 (sensitivity of 50 eggs/g). Immediately after homogenising, 0.5 mL aliquots of the solution were added to both chambers of a McMaster slide. At ten magnifications, parasite eggs were counted within each slide chamber under a light microscope. The number of eggs on the slide was then added and multiplied by 15 to obtain the eggs per gram for each sample. Upon observation of cyathostomin eggs during FEC analysis, the remaining faecal aliquots were subjected to larval culture to profile the nemabiome.

None of the horses demonstrated any signs of colic when observed over 24 h following anthelmintic administration. Faecal consistency and feed intake also remained standard for these animals following treatment.

Cyathostomin larval culture

Faecal samples were weighed and mixed with 30% vermiculite for incubation in a culture chamber (25°C and 60% humidity) to allow cyathostomin eggs to hatch and develop into L3 larvae. The faeces were stirred and moistened as needed for 12 days before the larvae were recovered using the Baermann technique. Faeces of the treated horses were cultured before treatment and on a weekly basis after the expected faecal egg reappearance period from day 28 to day 42. They were matched with that of the untreated ponies.

Microorganisms and cyathostomin larval DNA extraction from faecal samples

For the microbiota profiling, total DNA extraction from the 520 samples was performed as previously described [19]. DNA was extracted from 200 mg of faecal material using the EZNA Stool DNA Kit (Omega

Bio-Tek, Norcross, Georgia, USA). According to the manufacturer's instructions, the DNA extraction protocol was carried out (Omega Bio-Tek, Norcross, Georgia, USA). The DNA was then quantified using a Qubit and a dsDNA HS assay kit (Thermo Fisher).

Cyathostomin larval samples were incubated for one day and overnight at 57°C in lysis buffer (48 µL NaCl (1M), 6 µL Tris-HCl (pH 8.5; 1M), 120 µL EDTA (pH 8.0; 0.5M), 426 µL H20 RNase free, and 30 µL proteinase K solution). After the proteinase K digestion, 5 µL of RNAse solution was added and incubated for 1 h at 37°C. Then, 550 µL of phenol: chloroform: isoamyl alcohol (25:24:1) was added before centrifuging for 15 min at 14,000G in phase-lock tubes. The supernatant was then collected in a 1.5 ml tube, and 200 µL of chloroform was added and centrifuged again for 15 min at 14 000 G. The supernatant was again collected in a new tube, and 0.1X volume of 3M sodium acetate, 3X 100% ethanol and 2µL of pellet paint were added. Each sample was incubated at -20°C overnight. After incubation, a 30 min centrifugation at 14 000 G was performed. The supernatant was discarded, and 500 µL of alcohol was added to wash the pellet and centrifuged again (step performed twice). The sample was then air-dried (about 2 h) before being suspended in 30 µL of Tri-HCl.

V3–V4 16S rRNA and cyathostomin ITS-2 barcodes amplification

The bacterial V3-V4 hyper-variable regions of the 16S rRNA gene were amplified with two rounds of PCR as previously reported [19]. We added four negative controls during PCR cycles, two at PCR1 and two at PCR2, to control any source of contamination.

For cyathostomins, the ITS-2 region was PCR amplified using the NC1 and NC2 primers [82] as described previously [83]. A negative control sample and five distinct mock communities were added to establish putative biases in cyathostomin presence or absence [83]. In every case, the concentrations of the purified amplicons were checked using a NanoDrop 8000 spectrophotometer (Thermo Fisher Scientific, Waltham, USA), and the quality of a set of amplicons was checked using DNA 7500 chips onto a Bioanalyzer 2100 (Agilent Technologies, Santa Clara, CA, USA). The negative control samples did not yield a band on the agarose gel, and the concentration of the purified amplicons was undetectable (< 1 ng/µL).

All libraries were pooled at an equimolar concentration to generate an equivalent number of raw reads with each library. The final pool had a diluted concentration of 5 nM to 20 nM and was used for sequencing. According to Illumina's protocol, amplicon libraries were mixed with 15% PhiX control. For this study, one sequencing run was performed using MiSeq 500 cycle reagent kit v3 (2 x 250 output; Illumina, USA).

ITS-2 barcode data preprocessing and inferences on community composition

Amplicon sequencing data were quality-trimmed using cutadapt [84] (v. 1.14) (with options –pair-filter any –no-indels -m 50 –max-n 1 -q 15 -n 2), and subsequently handled with the Divisive Amplicon Denoising Algorithm (DADA2) algorithm [85] implemented in the R (v. 4.0.2) software version. Errors were learned, and the reads denoised, tolerating a single error for each of the forward and reverse reads, with further filtering of reads shorter than 200 bp and setting the band size parameter to 32 as recommended for ITS-2 amplicons before additional chimaera removal. The amplicon sequence variant (ASV) taxonomy assignment was subsequently performed using the IDTAXA algorithm [86] as implemented in the DECIPHER (v. 2.18.1) R package, enabling a 50% bootstrap cutoff and using the public nematode ITS-2 database v1.3 (https://www.nemabiome.ca/its2-database.html, last accessed, February 3rd, 2022). The ASV count table was subsequently handled with the phyloseq [87] package (v. 1.34). A total of 345 ASVs were identified, of which 106 with less than 50 occurrences were deemed contaminant and removed, and 16 were not assigned to any genus or species. Nemabiome samples showing less than 30 counts (*n* = 11 and the negative control) were not considered further. ASVs were subsequently aggregated at the species level using the *tax_glom()* function of the phyloseq package and removing unassigned ASVs. This left 14 strongylid species and three genus-wise ASVs for 52 samples. As a result of pyrantel treatment, 16 samples were missing due to low or no parasite egg excretion in the treated groups. However, five and three additional samples of the untreated and treated groups also failed (details provided in Supplementary information; Fig S8-S10). To deal with this issue and to promote the study of interactions between bacterial genera and cyathostomin, species counts of the treated groups were set to 0 while that of the control group were assigned to species average abundance recorded in the remaining samples (*n* = 8 for day 35; *n* = 5 for day 42). In the end, nine and 10 individuals were available for the HIGH-CTL and HIGH-TRT groups.

Species assignment for *Enterococcus* genus

Species-level assignments were made by taking a consensus of BLAST results for each *Enterococcus* ASV. That is, sequences were BLAST-ed against *nt*, excluding uncultured/environmental accessions. The species designations of all BLAST hits sharing the top score were collated. If all top-hit species designations agreed, a species assignment was made. Accessions with no species designation were ignored.

Host blood transcriptomic

To characterise the host response to cyathostomin infection, parasite removal and parasite re-emergence, blood samples were taken (Tempus Blood RNA tubes, Thermo Fisher) from a subset of six individuals within each group at day 0, 24h and 42 days post-treatment to perform mRNA sequencing (Supplementary information). Total RNAs were then isolated using the Preserved Blood RNA Purification Kit I (Norgen Biotek Corp., Ontario, Canada), according to the manufacturer's instructions. RNA purity and concentration were determined using a NanoDrop ND-1000 spectrophotometer (Thermo Fisher), and RNA

integrity was assessed using a Bioanalyzer 2100 (Agilent Technologies, Santa Clara, CA, United States). Total RNAs were subjected to poly-A tail enrichment and library preparation following the Illumina Truseq Stranded mRNA recommendations and sequenced on a NovaSeq 6000 platform. Adapter sequences were removed using cutadapt (v. 3.4) [84], and reads were filtered with Trimmomatic (v. 0.36) [88] for a minimum length of 100 bp and minimum leading and trailing base quality of 20. Retained reads were subsequently processed with Salmon (v. 1.4) [89] for pseudo-mapping against the *Equus caballus* v3 reference transcriptome (Ensembl v. 103), correcting for GC (–gcBias), position (–posBias) and sequence (–seqBias) biases and enabling selective alignment (–validateMappings). RNAseq counts were regressed upon the variables of interest to establish their respective contribution to expression variance using the variancePartition package (v. 1.20) [90]. RNA counts were filtered to retain genes with log(cpm) > 1 and corrected to account for gene-wise dispersion trend across samples with the *voomWithDreamWeights()* function [90]. The variance was subsequently partitioned across the effect of time, treatment, the respective pair-wise interactions between these three factors, the time x condition interaction and inter-individual variation using the *fitExtractVarPartModel*. The same framework was applied to the subset of high shedders to isolate the genes most affected by treatment, time, and their interaction effects. To define the transcriptomic signature associated with each variable, we retained the top 5% genes with a higher contribution to the variance. For the genes of interest, linear regression of gene count upon the treatment and time effects and blocking for the random individual effect was applied with the lme4 package. For specific comparison between groups (between high and low-shedders on day 0, between treated and untreated high-shedders on day 1) and to avoid relying on a single analytical framework, gene counts were handled with the DESeq2 package [91]. Analyses were applied to genes with at least ten counts across *n* individuals, *n* referring to the least considered group size, *e.g.* 12 (infection effect at day 0) or six (any other comparisons). Gene expression levels were compared between high and low-shedders before treatment (*n* = 12 individuals in each group) to identify the impact of cyathostomin infection in the host. To retain the most discriminant genes, a π score [92] was computed as:

$$\pi = -log10(adjusted\ pvalue)\ x\ |log2(Fold\ change)|.$$

Gene set enrichment analysis was run with the g:profiler2 package [93], retaining enrichment with an adjusted *P*-value below 5%.

Faecal microbiota data preprocessing

The DADA was also implemented using the DADA2 plug-in for QIIME 2 (v. 2021.2) to perform quality filtering and chimaera removal and construct a feature table consisting of reads abundance per ASV by sample [85]. Taxonomic assignments were given to ASVs by importing both SILVA 16S rRNA full-length database (release 138; https://www.arb-silva.de/documentation/release-138/) and SILVA 16S rRNA region-specific (515F/806R) database (release 138, 99% identity; Silva 138 99% OTUs from 515F/806R region of sequences) to QIIME 2 and classifying representative ASVs using the naive Bayes classifier plug-in [94]. The full-length and region-specific annotation tables were combined, avoiding redundancy.

Subsequently, for each ASV with an unidentified genus, homology-based identifications were performed using blast (v. 2.9.0) on the NCBI 16S ribosomal RNA reference database (released on May 25th, 2020) containing 20 845 sequences belonging to archaea and bacteria for classification in Greedy run mode allowing for maximum three mismatches with an E-value smaller than $1e^{-8}$.

The feature table, taxonomy, and phylogenetic tree were exported from QIIME 2 to the R statistical environment (v. 4.1.0) and combined into a phyloseq object using the phyloseq R package (v. 1.36.0) [87]. The ASV counts per sample and ASV taxonomic assignments are available in Table S2. Abundance data were aggregated at genus, family, order, class, and phyla using the *tax_glom()* function of the phyloseq R package.

Microbiota biodiversity and richness analysis: core genera, α- and β-diversity

The core genera, cross-sectional genera found at every time point and individuals, were estimated using a detection threshold of 0.1% and a prevalence threshold of 95% in the microbiome R package (v. 1.15.3; http://microbiome.github.io).

This microbiome R package produced the measures of evenness, dominance, divergences, and abundance. The gut α-diversity indices between groups and time points were compared using a generalised linear model (*glmer()* function of the lme4 package (v. 1.1-27.1)), where the group, day, faecal pH, faecal DNA concentration, age, and the box were included as fixed effects and individuals as a random effect.

Bray-Curtis dissimilarity and unweighted and weighted UniFrac distances were calculated using the phyloseq R package to estimate β-diversity. For this, samples were rarefied at 16 875 reads of depth (minimum sampling depth in our data) to allow an equal depth using the *rarefy_even_depth()* function of the phyloseq R package. The minimal sequencing depth was sufficient for accurately profiling bacterial composition, as predicted by calculating the rarefaction curve for observed richness, Chao1, and Shannon index (which accounts for both abundance and evenness; Supplementary information). The β-diversity was visualised using the non-metric dimensional scaling (NMDS) in the vegan R package (v. 2.5.7) [95] using the *metaMDS()* function. The stress value was calculated to determine the dimensions for each NMDS. The partitioning of β-diversity into turnover (β_{TURN}) and nestedness (β_{NEST}) components was performed with the betapart R package (v. 1.5.6) [96].

The PerMANOVA test (a non-parametric method of multivariate analysis of variance based on pairwise distances) implemented in the *adonis2*() function from the vegan (v. 2.5.7) [95] R package allowed testing of the global association between ecological community structure and groups across time. The strata option (strata = horse) was used to account for repeated sampling of individual horses. Specifically, we tested the effects of group and time corrected by age, faecal pH, faecal DNA

concentration, and the box on the variation of total dissimilarity between faecal microbiota. The significance of the effect of group and time was assessed in an F-test based on the sequential sum of squares estimated from a 10 000 permutations procedure. The significance threshold was chosen at an adjusted $P < 0.05$.

Pairwise comparisons of mean Bray–Curtis distances to group centroids among horse faecal samples were calculated using the permutational analysis of multivariate dispersion, *permdisp()* function in vegan package.

In addition to multivariate analysis, we used the analysis of similarities (ANOSIM) to test for intragroup dispersion. ANOSIM is a permutation-based test where the null hypothesis states that within-group distances are not significantly smaller than between-group distances. The test statistic (R) can range from 1 to −1, with a value of 1 indicating that all samples within groups are more similar than any other representatives from different groups. R is ≈ 0 when the null hypothesis is true, that distances within and between groups are the same on average. Because multiple comparison corrections for ANOSIM were unavailable, the number of permutations used on those calculations increased to 9 999.

The effect size of the host and environmental variables on the ASV level community ordination was tested using the *envfit()* function in the vegan R package (10,000 permutations, Benjamini-Hochberg adjusted $P < 0.05$). The *envfit()* function performs multivariate analysis of variance (MANOVA) and linear correlations for categorical and continuous variables. The effect size and significance of each covariate were determined by comparing the difference in the centroids of each group relative to the total variation. The obtained r^2 gives the proportion of variability (that is, the main dimensions of the ordination) that can be attributed to the explanatory variables. Complementary, we employed the variation partitioning analysis *varpart()* function in the R package vegan to account for direct and indirect effects of environmental factors, where dissimilarities in faecal microbiota composition were considered as a response and divergence in host and environmental factors.

Microbial homogeneity across groups and time

The homogeneity of dispersions of microbiota composition between groups and time points was tested through Whittaker's index using the multivariate analyses of the homogeneity of group dispersion, that is, the distance of individual groups from the centroid of their group. The *betadisper()* function of the Vegan R package was employed. Moreover, to assess whether the within- and between-group variability in beta diversity were compared for each group separately through an ANOVA test on the group dispersions using the *aov()* function in R followed by the post hoc Tukey-Kramer at 0.95 and the multiple-test correction of Benjamini-Hochberg (adj $P < 0.05$).

The contribution of each genus to the ecosystem temporal dynamics through groups

MaAsLin 2 R package (v. 1.8.0) [97], a multivariate statistical framework utilising generalised linear models, was used to analyse the effect of group and time points jointly with associated covariates on genera abundances, allowing formulation of both fixed effects and random effects (for within-subject correlations) in a single unified framework. Age was not considered a potential confounding factor in the MaAsLin analyses. Multiple time points per subject were considered by including the subject in the model as random effects. MaAsLin transformed the raw abundance of each genus with an arcsine square root transformation before testing for associations. The FDR threshold was set at adjusted $P < 0.05$ for all MaAsLin tests, with boosting and quality control steps enabled.

Intraclass correlation coefficient

The intraclass correlation coefficient (ICC) estimation uses the variance components from a one-way ANOVA (among-group variance and within-group variance; ICC = $variance_{between}$/[$variance_{between}$ + $variance_{within}$]). Here, the ICC was calculated based on the longitudinal genera abundance, defining each group as a distinct class, using a linear mixed-effects model (lme4; v. 1.1.28 R package) with day fitted as a fixed effect and horse as a random effect to account for inter-horse variation, as applied in the function *ICC()* of the sjmisc (v. 2.8.9) R package. Inter- and intra-subject variation was estimated using all individuals within each experimental group. Higher the ICC value, the higher the correlation between time points. Moreover, conditional (R^2c) and marginal (R^2m) coefficients of determination were calculated using the function *r.squaredGLMM()* in the R package lme4. The model's marginal R^2_m represents the variance explained by fixed effects, whereas the conditional R^2_c accounts for the variance explained by fixed and random effects combined.

Quantification of the prediction of response

The receiver operating characteristics (ROC) and precision-recall analyses were performed using the R package pROC (v. 1.18.0) package to quantify the infection status predictive power of the gut microbiota. Recall and precision were essential metrics for metagenomic classification [98]. The ROCit R package (v. 2.1.1) was employed to plot the ROC curve, and from this, it calculated an optimal cut-off was determined by the Youden method.

Pyrantel treatment effect on cyathostomin community: differential abundance analysis and multi-spatial Convergent cross-mapping (CCM)

Pyrantel efficacy was estimated from the Faecal Egg Count Reduction 14 days after pyrantel treatment [99] using the eggCounts package [100]. Egg Reappearance Period (ERP) in ponies' faeces was

considered the day when observed FEC reduction fell below 90% of that measured at 14 days post-treatment [99].

To investigate the pyrantel treatment effect on the cyathostomin community, we first focused on the difference in community composition observed on day 0 and day 42 after treatment, using available data from five untreated and seven treated ponies. Alpha diversity coefficients (estimated with the *estimate_richness()* function of the phyloseq package) were compared between the two-time points within each group using a *t*-test. The group and day effects were estimated using a PerMANOVA on Jaccard distance on species presence/absence and Bray-Curtis dissimilarity on relative abundances (using the *ordinate()* function of the phyloseq package), using the *adonis2()* function of the vegan package (1 000 permutations and accounting for pony effect using the strata option). To isolate species with significant variation in abundance between the two timepoints, count data were modelled using the DESeq2 package for the same 12 samples. This analysis was restricted to 15 species found in at least four individuals and with more than 50 counts to avoid convergence issues.

To establish how pyrantel was affecting species interaction, we inferred causal relationships between measured FEC, faecal pH and 43 faecal microbiota genera (with more than 20 000 counts; 93.8% of total abundance) using the multi-spatial Convergent Cross-Mapping (CCM) procedure [101]. This extension of the classical CCM [36] leverages a bootstrapping approach to infer the causative effect of one interactor on the other from their respective replicated time series [101]. As such, it is well adapted to shorter time series (less than 30-time points). For this analysis, the time-series data consisted of the replicate observations (n = 20 horses in the treated or untreated groups) gathered on day 0 and the weekly collected data after the expected egg reappearance period (days 28, 35, and 42) as parasites were not expected to re-appear before 28 days after treatment. Therefore, the considered time lag was uneven between the first and second observations a month apart, and this analysis implicitly assumed a steady state between day 0 and day 28. This assumption was considered conservative as variations observed in the untreated ponies may reduce the ability to detect relationships between bacteria and parasite species. In the treated individuals, the transition between day 0 and day 28 is the only one being informative about the system states. The best embedding value E, *e.g.* the number of past time lags used to predict the next value, was determined after examining the predictability obtained considering two or three historical records. The significance of the interaction was tested with 1 000 bootstraps retaining correlation with a P-value below 5%. This procedure was run on the treated and untreated groups separately.

Stability of the gut microbiota community following disturbance (pyrantel treatment)

Dynamic stability is an aggregated measure of the stability of a species interaction matrix across time, whose value distinguishes between unstable communities (stability > 1) or more stable assemblage (stability < 1) [102]. To establish how pyrantel treatment rewired the interaction network of bacterial species, we estimated the dynamic stability of the gut microbiota collected from the 20 treated and 20

untreated individuals following a previously described approach [102]. We first isolated the interacting major bacterial genera (43 taxa represented by more than 20 000 counts and amounting to 93.8% of total sequences) using the multispatial CCM package [101], varying embedding from 2 to 7 and retaining the value with maximal predictability. After 1 000 bootstraps, species pairs showing significant predictability (correlation above the 95% confidence interval upper limit) and convergence (difference between correlation estimated with the smallest and largest library size above 0.1) were deemed to have significant interaction with each other (n = 151 distinct pairs between 43 genera) [101]. Species interaction strengths between these pairs were subsequently derived at each time point using the multivariate S-map method [103]. This method produces weighted multivariate linear regression models that predict the future interaction values between one species and its interactant using past observed interactions in the time series. S-maps hence model a given species abundance at time $t + 1$ as the sum of an intercept and partial derivatives (interaction strength) of that species abundance with its interactant abundances at the time t [101]. In this respect, the number of partial derivatives must equal the best embedding E determined from CCM for that species. As a result, time lags of that species were used as a replacement when the number of interactant species was lower than E, as described previously [102]. The community dynamics can thus be summarised in an interaction strength matrix (partial derivative matrix) whose dominant eigenvalue (absolute value of its real part) corresponds to the dynamic stability [102]. S-maps were estimated with the rEDM (v. 0.7.5) R package [104], and eigenvalues were estimated as described previously [102]. This workflow was applied separately to the gut microbiota of the treated (n = 20) and untreated ponies (n = 20), yielding the dynamic stability coefficients associated with each of the 40 bacterial communities. As empirical dynamic modelling relies on evenly spaced time series, this analysis was restricted to the weekly observations, ignoring the six-time points collected during the first three days post-treatment.

DATA AVAILABILITY

The gut metagenome 16S rRNA targeted locus data are available in the DDBJ/EMBL/GenBank under the BioProject PRJNA438436 and accessions from SRR18489300 to SRR18489819. The accession numbers of the BioSamples included here are SAMN26941952 to SAMN26942471. The nemabiome data used in this paper spanned BioSamples SAMN29052217 to SAMN29052295 of the SRA BioProject PRJNA849212. RNAseq data have been released as part of the BioProject PRJNA849212.

Data sets and products generated from the raw sequence data are available at the INRAE institutional data repository powered by Dataverse with DOI: https://doi.org/10.57745/AS7NTU. The validation set data are available under BioProject PRJEB39250, PRJNA433202, ERP118335, and at http://doi.org/10.17632/g7chkjrp8f.1.

All other data is available in the Supplementary Data.

CODE AVAILABILITY

The R-scripts used are available at the INRAE institutional data repository powered by Dataverse with DOI with public access: https://doi.org/10.57745/AS7NTU.

Declarations

AUTHOR CONTRIBUTIONS

GS and NM conceived the study. MB and SP performed all DNA extractions. MB performed the 16S rRNA bioinformatics data analyses and estimated the microbiota diversity under the supervision of NM. GS and SP performed RNA extraction. JL and GA sequenced the libraries. GS designed and performed the nemabiome bioinformatics, biostatistics, and stability analysis. NM performed 16S rRNA statistical analyses. DB performed the 16S rRNA PCRs. DS, MB and FR organised the sample collection and carried out the faecal egg counts and the larval culture. GA, CK, SP, EC, and GS prepared the microbiome and nemabiome sequencing libraries. AG and FR were responsible for pony maintenance and care throughout the experiment. GS and NM wrote the manuscript. All authors read and approved the final manuscript.

COMPETING INTERESTS

The authors declare no competing interests.

FINANCIAL SUPPORT

This work was funded by grants from the Institut Français du Cheval et de l'Equitation (IFCE), the Fonds Éperon and the Institute National de la Recherche pour l'Agriculture, l'alimentation et l'environnement (INRAE).

ACKNOWLEDGMENTS

We are grateful to Yvan Gaude, Thierry Blard, and Philippe Barrière for participating in the sample collection and organisation during the project. We are grateful to the genotoul bioinformatics facility (Bioinfo Genotoul, https://doi.org/10.15454/1.5572369328961167E12; Toulouse, France) and MIGALE bioinformatics facility (https://doi.org/10.15454/1.5572390655343293E12; Jouy en Josas, France) for providing help, computing, and storage resources.

References

1. Rynkiewicz EC, Pedersen AB, Fenton A. An ecosystem approach to understanding and managing within-host parasite community dynamics. Trends in Parasitology 2015; **31**: 212–221.
2. Hayes KS, Bancroft AJ, Goldrick M, Portsmouth C, Roberts IS, Grencis RK. Exploitation of the intestinal microflora by the parasitic nematode Trichuris muris. Science 2010; **328**: 1391–4.
3. Reynolds LA, Smith KA, Filbey KJ, Harcus Y, Hewitson JP, Redpath SA, et al. Commensal-pathogen interactions in the intestinal tract: lactobacilli promote infection with, and are promoted by, helminth

parasites. Gut microbes 2014; **5**: 522–32.

4. Reynolds LA, Finlay BB. Worming Their Way into the Picture: Microbiota Help Helminths Modulate Host Immunity. Immunity 2015; **43**: 840–842.
5. Leung JM, Graham AL, Knowles SCL. Parasite-Microbiota Interactions With the Vertebrate Gut: Synthesis Through an Ecological Lens. Front Microbiol 2018; **9**: 843.
6. Cooper P, Walker AW, Reyes J, Chico M, Salter SJ, Vaca M, et al. Patent human infections with the whipworm, Trichuris trichiura, are not associated with alterations in the faecal microbiota. PLoS One 2013; **8**: e76573.
7. Lee SC, Tang MS, Lim YAL, Choy SH, Kurtz ZD, Cox LM, et al. Helminth Colonization Is Associated with Increased Diversity of the Gut Microbiota. *Plos Neglect Trop D* 2014; **8**.
8. Jenkins TP, Rathnayaka Y, Perera PK, Peachey LE, Nolan MJ, Krause L, et al. Infections by human gastrointestinal helminths are associated with changes in faecal microbiota diversity and composition. PLoS ONE 2017; **12**: e0184719.
9. Aivelo T, Norberg A. Parasite-microbiota interactions potentially affect intestinal communities in wild mammals. J Anim Ecol 2018; **87**: 438–447.
10. Newbold LK, Burthe SJ, Oliver AE, Gweon HS, Barnes CJ, Daunt F, et al. Helminth burden and ecological factors associated with alterations in wild host gastrointestinal microbiota. ISME J 2017; **11**: 663–675.
11. Knowles SCL, Fenton A, Petchey OL, Jones TR, Barber R, Pedersen AB. Stability of within-host–parasite communities in a wild mammal system. Proc R Soc B 2013; **280**: 20130598.
12. Kreisinger J, Bastien G, Hauffe HC, Marchesi J, Perkins SE. Interactions between multiple helminths and the gut microbiota in wild rodents. Phil Trans R Soc B 2015; **370**: 20140295.
13. Ling F, Steinel N, Weber J, Ma L, Smith C, Correa D, et al. The gut microbiota response to helminth infection depends on host sex and genotype. ISME J 2020; **14**: 1141–1153.
14. Wu S, Li RW, Li W, Beshah E, Dawson HD, Urban JF. Worm burden-dependent disruption of the porcine colon microbiota by Trichuris suis infection. PLoS One 2012; **7**: e35470.
15. Li RW, Wu S, Li W, Navarro K, Couch RD, Hill D, et al. Alterations in the porcine colon microbiota induced by the gastrointestinal nematode Trichuris suis. Infection and immunity 2012; **80**: 2150–7.
16. Cortés A, Wills J, Su X, Hewitt RE, Robertson J, Scotti R, et al. Infection with the sheep gastrointestinal nematode Teladorsagia circumcincta increases luminal pathobionts. Microbiome 2020; **8**: 60.
17. Li RW, Wu S, Li W, Huang Y, Gasbarre LC. Metagenome plasticity of the bovine abomasal microbiota in immune animals in response to Ostertagia ostertagi infection. PLoS One 2011; **6**: e24417.
18. Li RW, Li W, Sun J, Yu P, Baldwin RL, Urban JF. The effect of helminth infection on the microbial composition and structure of the caprine abomasal microbiome. Sci Rep 2016; **6**: 20606.
19. Clark A, Sallé G, Ballan V, Reigner F, Meynadier A, Cortet J, et al. Strongyle Infection and Gut Microbiota: Profiling of Resistant and Susceptible Horses Over a Grazing Season. Frontiers in Physiology 2018; **9**.

20. Peachey LE, Molena RA, Jenkins TP, Di Cesare A, Traversa D, Hodgkinson JE, et al. The relationships between faecal egg counts and gut microbial composition in UK Thoroughbreds infected by cyathostomins. Int J Parasitol 2018; **48**: 403–412.
21. Walshe N, Duggan V, Cabrera-Rubio R, Crispie F, Cotter P, Feehan O, et al. Removal of adult cyathostomins alters faecal microbiota and promotes an inflammatory phenotype in horses. Int J Parasitol 2019; **49**: 489–500.
22. Kunz IGZ, Reed KJ, Metcalf JL, Hassel DM, Coleman RJ, Hess TM, et al. Equine Fecal Microbiota Changes Associated With Anthelmintic Administration. J Equine Vet Sci 2019; **77**: 98–106.
23. Daniels SP, Leng J, Swann JR, Proudman CJ. Bugs and drugs: a systems biology approach to characterising the effect of moxidectin on the horse's faecal microbiome. anim microbiome 2020; **2**: 38.
24. Ramanan D, Bowcutt R, Lee SC, Tang MS, Kurtz ZD, Ding Y, et al. Helminth infection promotes colonization resistance via type 2 immunity. Science 2016; **352**: 608–612.
25. Rosa BA, Snowden C, Martin J, Fischer K, Kupritz J, Beshah E, et al. Whipworm-Associated Intestinal Microbiome Members Consistent Across Both Human and Mouse Hosts. Front Cell Infect Microbiol 2021; **11**: 637570.
26. Schachter J, Alvarinho de Oliveira D, da Silva CM, de Barros Alencar ACM, Duarte M, da Silva MMP, et al. Whipworm Infection Promotes Bacterial Invasion, Intestinal Microbiota Imbalance, and Cellular Immunomodulation. Infect Immun 2020; **88**: e00642-19.
27. Fricke WF, Song Y, Wang A-J, Smith A, Grinchuk V, Pei C, et al. Type 2 immunity-dependent reduction of segmented filamentous bacteria in mice infected with the helminthic parasite Nippostrongylus brasiliensis. Microbiome 2015; **3**: 40.
28. Holm JB, Sorobetea D, Kiilerich P, Ramayo-Caldas Y, Estelle J, Ma T, et al. Chronic Trichuris muris Infection Decreases Diversity of the Intestinal Microbiota and Concomitantly Increases the Abundance of Lactobacilli. PLoS One 2015; **10**: e0125495.
29. Peachey LE, Jenkins TP, Cantacessi C. This Gut Ain't Big Enough for Both of Us. Or Is It? Helminth-Microbiota Interactions in Veterinary Species. Trends Parasitol 2017; **33**: 619–632.
30. Cortés A, Toledo R, Cantacessi C. Classic Models for New Perspectives: Delving into Helminth-Microbiota-Immune System Interactions. Trends Parasitol 2018; **34**: 640–654.
31. Coyte KZ, Rakoff-Nahoum S. Understanding Competition and Cooperation within the Mammalian Gut Microbiome. Curr Biol 2019; **29**: R538–R544.
32. Coyte KZ, Schluter J, Foster KR. The ecology of the microbiome: Networks, competition, and stability. Science 2015; **350**: 663–666.
33. May RM. Will a Large Complex System be Stable? Nature 1972; **238**: 413–414.
34. McNally L, Brown SP. Microbiome: Ecology of stable gut communities. Nat Microbiol 2016; **1**: 15016.
35. McClemens J, Kim JJ, Wang H, Mao YK, Collins M, Kunze W, et al. Lactobacillus rhamnosus ingestion promotes innate host defense in an enteric parasitic infection. Clinical and vaccine

immunology: CVI 2013; **20**: 818–26.

36. Sugihara G, May R, Ye H, Hsieh C, Deyle E, Fogarty M, et al. Detecting causality in complex ecosystems. Science 2012; **338**: 496–500.
37. Afrin T, Murase K, Kounosu A, Hunt VL, Bligh M, Maeda Y, et al. Sequential Changes in the Host Gut Microbiota During Infection With the Intestinal Parasitic Nematode Strongyloides venezuelensis. Front Cell Infect Microbiol 2019; **9**: 217.
38. Houlden A, Hayes KS, Bancroft AJ, Worthington JJ, Wang P, Grencis RK, et al. Chronic Trichuris muris Infection in C57BL/6 Mice Causes Significant Changes in Host Microbiota and Metabolome: Effects Reversed by Pathogen Clearance. PLoS ONE 2015; **10**: e0125945.
39. Gaulke CA, Martins ML, Watral VG, Humphreys IR, Spagnoli ST, Kent ML, et al. A longitudinal assessment of host-microbe-parasite interactions resolves the zebrafish gut microbiome's link to Pseudocapillaria tomentosa infection and pathology. Microbiome 2019; **7**: 10.
40. Wootton JT, Emmerson M. Measurement of Interaction Strength in Nature. Annu Rev Ecol Evol Syst 2005; **36**: 419–444.
41. Pedersen AB, Antonovics J. Anthelmintic treatment alters the parasite community in a wild mouse host. Biol Lett 2013; **9**: 20130205.
42. Budischak SA, Hoberg EP, Abrams A, Jolles AE, Ezenwa VO. Experimental insight into the process of parasite community assembly. J Anim Ecol 2016; **85**: 1222–1233.
43. Yang C-A, Liang C, Lin C-L, Hsiao C-T, Peng C-T, Lin H-C, et al. Impact of Enterobius vermicularis infection and mebendazole treatment on intestinal microbiota and host immune response. PLoS Negl Trop Dis 2017; **11**: e0005963.
44. Ogbourne CP. The prevalence, relative abundance and site distribution of nematodes of the subfamily Cyathostominae in horses killed in Britain. J Helminthol 1976; **50**: 203–14.
45. Bucknell DG, Gasser RB, Beveridge I. The prevalence and epidemiology of gastrointestinal parasites of horses in Victoria, Australia. Int J Parasitol 1995; **25**: 711–24.
46. Kuzmina TA, Kharchenko VA, Starovir AI, Dvojnos GM. Analysis of the strongylid nematodes (Nematoda: Strongylidae) community after deworming of brood horses in Ukraine. Vet Parasitol 2005; **131**: 283–90.
47. Ang L, Vinderola G, Endo A, Kantanen J, Jingfeng C, Binetti A, et al. Gut Microbiome Characteristics in feral and domesticated horses from different geographic locations. Commun Biol 2022; **5**: 172.
48. Gilroy R, Leng J, Ravi A, Adriaenssens EM, Oren A, Baker D, et al. Metagenomic investigation of the equine faecal microbiome reveals extensive taxonomic diversity. PeerJ 2022; **10**: e13084.
49. Mach N, Midoux C, Leclercq S, Pennarun S, Le Moyec L, Rué O, et al. The first horse gut microbiome gene catalog reveals that rare microbiome ensures better cardiovascular fitness in endurance horses. 2022. Microbiology.
50. Plancade S, Clark A, Philippe C, Helbling J-C, Moisan M-P, Esquerré D, et al. Unraveling the effects of the gut microbiota composition and function on horse endurance physiology. Sci Rep 2019; **9**: 9620.

51. Stewart HL, Pitta D, Indugu N, Vecchiarelli B, Engiles JB, Southwood LL. Characterization of the fecal microbiota of healthy horses. Am J Vet Res 2018; **79**: 811–819.
52. O' Donnell MM, Harris HMB, Jeffery IB, Claesson MJ, Younge B, O' Toole PW, et al. The core faecal bacterial microbiome of Irish Thoroughbred racehorses. Lett Appl Microbiol 2013; **57**: 492–501.
53. Olsson LM, Boulund F, Nilsson S, Khan MT, Gummesson A, Fagerberg L, et al. Dynamics of the normal gut microbiota: A longitudinal one-year population study in Sweden. Cell Host & Microbe 2022; **30**: 726–739.e3.
54. Nielsen MK, Betancourt A, Lyons ET, Horohov DW, Jacobsen S. Characterization of the inflammatory response to anthelmintic treatment of ponies with cyathostominosis. Vet J 2013; **198**: 457–62.
55. Pasolli E, De Filippis F, Mauriello IE, Cumbo F, Walsh AM, Leech J, et al. Large-scale genome-wide analysis links lactic acid bacteria from food with the gut microbiome. Nat Commun 2020; **11**: 2610.
56. Hou K, Wu Z-X, Chen X-Y, Wang J-Q, Zhang D, Xiao C, et al. Microbiota in health and diseases. Sig Transduct Target Ther 2022; **7**: 135.
57. Daniels SP, Leng J, Swann JR, Proudman CJ. Bugs and drugs: a systems biology approach to characterising the effect of moxidectin on the horse's faecal microbiome. Animal Microbiome 2020; **2**: 38.
58. White EC, Houlden A, Bancroft AJ, Hayes KS, Goldrick M, Grencis RK, et al. Manipulation of host and parasite microbiotas: Survival strategies during chronic nematode infection. Sci Adv 2018; **4**: eaap7399.
59. Atarashi K, Tanoue T, Oshima K, Suda W, Nagano Y, Nishikawa H, et al. Treg induction by a rationally selected mixture of Clostridia strains from the human microbiota. Nature 2013; **500**: 232–236.
60. Atarashi K, Tanoue T, Shima T, Imaoka A, Kuwahara T, Momose Y, et al. Induction of Colonic Regulatory T Cells by Indigenous *Clostridium* Species. Science 2011; **331**: 337–341.
61. Parada Venegas D, De la Fuente MK, Landskron G, González MJ, Quera R, Dijkstra G, et al. Short Chain Fatty Acids (SCFAs)-Mediated Gut Epithelial and Immune Regulation and Its Relevance for Inflammatory Bowel Diseases. Front Immunol 2019; **10**: 277.
62. Heinken A, Ravcheev DA, Baldini F, Heirendt L, Fleming RMT, Thiele I. Systematic assessment of secondary bile acid metabolism in gut microbes reveals distinct metabolic capabilities in inflammatory bowel disease. Microbiome 2019; **7**: 75.
63. Lindenberg F, Krych L, Fielden J, Kot W, Frøkiær H, van Galen G, et al. Expression of immune regulatory genes correlate with the abundance of specific Clostridiales and Verrucomicrobia species in the equine ileum and cecum. Scientific Reports 2019; **9**: 1–10.
64. Rafaluk-Mohr C, Gerth M, Sealey JE, Ekroth AKE, Aboobaker AA, Kloock A, et al. Microbial protection favors parasite tolerance and alters host-parasite coevolutionary dynamics. Current Biology 2022; **32**: 1593–1598.e3.
65. Lin C-H, Chen M-C, Lin L-L, Christian DA, Min B, Hunter CA, et al. Gut epithelial IL-27 confers intestinal immunity through the induction of intraepithelial lymphocytes. J Exp Med 2021; **218**: e20210021.

66. Kooyman FN, van Doorn DC, Geurden T, Mughini-Gras L, Ploeger HW, Wagenaar JA. Species composition of larvae cultured after anthelmintic treatment indicates reduced moxidectin susceptibility of immature Cylicocyclus species in horses. Vet Parasitol 2016; **227**: 77–84.
67. Xiao L, Herd RP, Majewski GA. Comparative efficacy of moxidectin and ivermectin against hypobiotic and encysted cyathostomes and other equine parasites. Vet Parasitol 1994; **53**: 83–90.
68. Hu D, Chao Y, Zhang B, Wang C, Qi Y, Ente M, et al. Effects of Gasterophilus pecorum infestation on the intestinal microbiota of the rewilded Przewalski's horses in China. PLoS ONE 2021; **16**: 1–19.
69. Walshe N, Duggan V, Cabrera-Rubio R, Crispie F, Cotter P, Feehan O, et al. Removal of adult cyathostomins alters faecal microbiota and promotes an inflammatory phenotype in horses. International Journal for Parasitology 2019; **49**: 489–500.
70. Peachey LE, Molena RA, Jenkins TP, Di Cesare A, Traversa D, Hodgkinson JE, et al. The relationships between faecal egg counts and gut microbial composition in UK Thoroughbreds infected by cyathostomins. International Journal for Parasitology 2018; **48**: 403–412.
71. Martin I, Djuardi Y, Sartono E, Rosa BA, Supali T, Mitreva M, et al. Dynamic changes in human-gut microbiome in relation to a placebo-controlled anthelminthic trial in Indonesia. PLoS Negl Trop Dis 2018; **12**: e0006620.
72. Zaneveld JR, McMinds R, Vega Thurber R. Stress and stability: applying the Anna Karenina principle to animal microbiomes. Nat Microbiol 2017; **2**: 17121.
73. Fassarella M, Blaak EE, Penders J, Nauta A, Smidt H, Zoetendal EG. Gut microbiome stability and resilience: elucidating the response to perturbations in order to modulate gut health. Gut 2021; **70**: 595–605.
74. Faith JJ, Guruge JL, Charbonneau M, Subramanian S, Seedorf H, Goodman AL, et al. The long-term stability of the human gut microbiota. Science 2013; **341**: 1237439.
75. Dai W, Chen J, Xiong J. Concept of microbial gatekeepers: Positive guys? Appl Microbiol Biotechnol 2019; **103**: 633–641.
76. Williams AR, Peña-Espinoza MA, Boas U, Simonsen HT, Enemark HL, Thamsborg SM. Anthelmintic activity of chicory (Cichorium intybus): in vitro effects on swine nematodes and relationship to sesquiterpene lactone composition. Parasitology 2016; **143**: 770–777.
77. Schneeberger PHH, Gueuning M, Welsche S, Hürlimann E, Dommann J, Häberli C, et al. Different gut microbial communities correlate with efficacy of albendazole-ivermectin against soil-transmitted helminthiases. Nat Commun 2022; **13**: 1063.
78. PAO. Animal Physiology Facility. 2018.
79. Sallé G, Canlet C, Cortet J, Koch C, Malsa J, Reigner F, et al. Integrative biology defines novel biomarkers of resistance to strongylid infection in horses. Sci Rep 2021; **11**: 14278.
80. Gokbulut C, Nolan AM, Mckellar QA. Pharmacokinetic disposition and faecal excretion of pyrantel embonate following oral administration in horses. J Vet Pharmacol Ther 2001; **24**: 77–79.

81. Raynaud JP. [Study of the efficiency of a quantitative coproscopic technic for the routine diagnosis and control of parasitic infestations of cattle, sheep, horses and swine]. Ann Parasitol Hum Comp 1970; **45**: 321–42.
82. Gasser RB, Chilton NB, Hoste H, Beveridge I. Rapid sequencing of rDNA from single worms and eggs of parasitic helminths. Nucleic Acids Res 1993; **21**: 2525–2526.
83. Courtot E, Boisseau M, Dhorne-Pollet S, Serreau D, Gesbert A, Reigner F, et al. Evaluation of the nemabiome approach for the study of equine strongylid communities. 2022. Ecology.
84. Martin M. Cutadapt removes adapter sequences from high-throughput sequencing reads. EMBnet.journal 2011; **17**: 10.
85. Callahan BJ, McMurdie PJ, Rosen MJ, Han AW, Johnson AJA, Holmes SP. DADA2: High-resolution sample inference from Illumina amplicon data. Nature Methods 2016; **13**: 581–583.
86. Murali A, Bhargava A, Wright ES. IDTAXA: a novel approach for accurate taxonomic classification of microbiome sequences. Microbiome 2018; **6**: 140.
87. McMurdie PJ, Holmes S. phyloseq: An R Package for Reproducible Interactive Analysis and Graphics of Microbiome Census Data. PLoS ONE 2013; **8**: e61217.
88. Bolger AM, Lohse M, Usadel B. Trimmomatic: a flexible trimmer for Illumina sequence data. Bioinformatics 2014; **30**: 2114–2120.
89. Patro R, Duggal G, Love MI, Irizarry RA, Kingsford C. Salmon provides fast and bias-aware quantification of transcript expression. Nat Methods 2017; **14**: 417–419.
90. Hoffman GE, Roussos P. Dream: powerful differential expression analysis for repeated measures designs. Bioinformatics 2021; **37**: 192–201.
91. Love MI, Huber W, Anders S. Moderated estimation of fold change and dispersion for RNA-seq data with DESeq2. Genome Biol 2014; **15**: 550.
92. Xiao Y, Hsiao T-H, Suresh U, Chen H-IH, Wu X, Wolf SE, et al. A novel significance score for gene selection and ranking. Bioinformatics 2014; **30**: 801–807.
93. Kolberg L, Raudvere U, Kuzmin I, Vilo J, Peterson H. gprofiler2 – an R package for gene list functional enrichment analysis and namespace conversion toolset g:Profiler. F1000Res 2020; **9**: ELIXIR-709.
94. Bokulich NA, Kaehler BD, Rideout JR, Dillon M, Bolyen E, Knight R, et al. Optimizing taxonomic classification of marker-gene amplicon sequences with QIIME 2's q2-feature-classifier plugin. Microbiome 2018; **6**: 90.
95. Oksanen J, Blanchet FG, Friendly M, Kindt R, Legendre P, McGlinn D, et al. vegan: Community Ecology Package. R package version 2.4-3. 2017.
96. Baselga A, Orme CDL. betapart: an R package for the study of beta diversity: *Betapart package*. Methods in Ecology and Evolution 2012; **3**: 808–812.
97. Mallick H, Rahnavard A, McIver LJ, Ma S, Zhang Y, Nguyen LH, et al. Multivariable association discovery in population-scale meta-omics studies. PLoS Comput Biol 2021; **17**: e1009442.

98. Ye SH, Siddle KJ, Park DJ, Sabeti PC. Benchmarking Metagenomics Tools for Taxonomic Classification. Cell 2019; **178**: 779–794.
99. Nielsen MK, von Samson-Himmelstjerna G, Kuzmina TA, van Doorn DCK, Meana A, Rehbein S, et al. World association for the advancement of veterinary parasitology (WAAVP): Third edition of guideline for evaluating the efficacy of equine anthelmintics. Veterinary Parasitology 2022; **303**: 109676.
100. Wang C, Torgerson PR, Kaplan RM, George MM, Furrer R. Modelling anthelmintic resistance by extending eggCounts package to allow individual efficacy. Int J Parasitol Drugs Drug Resist 2018; **8**: 386–393.
101. Clark AT, Ye H, Isbell F, Deyle ER, Cowles J, Tilman GD, et al. Spatial convergent cross mapping to detect causal relationships from short time series. Ecology 2015; **96**: 1174–1181.
102. Ushio M, Hsieh C, Masuda R, Deyle ER, Ye H, Chang C-W, et al. Fluctuating interaction network and time-varying stability of a natural fish community. Nature 2018; **554**: 360–363.
103. Deyle ER, May RM, Munch SB, Sugihara G. Tracking and forecasting ecosystem interactions in real time. Proc Biol Sci 2016; **283**: 20152258.
104. Ye H, Clark A, Deyle E, Munch S, Keyes O, Cai J, et al. Redm: Applications Of Empirical Dynamic Modeling From Time Series. 2018. Zenodo.

Figures

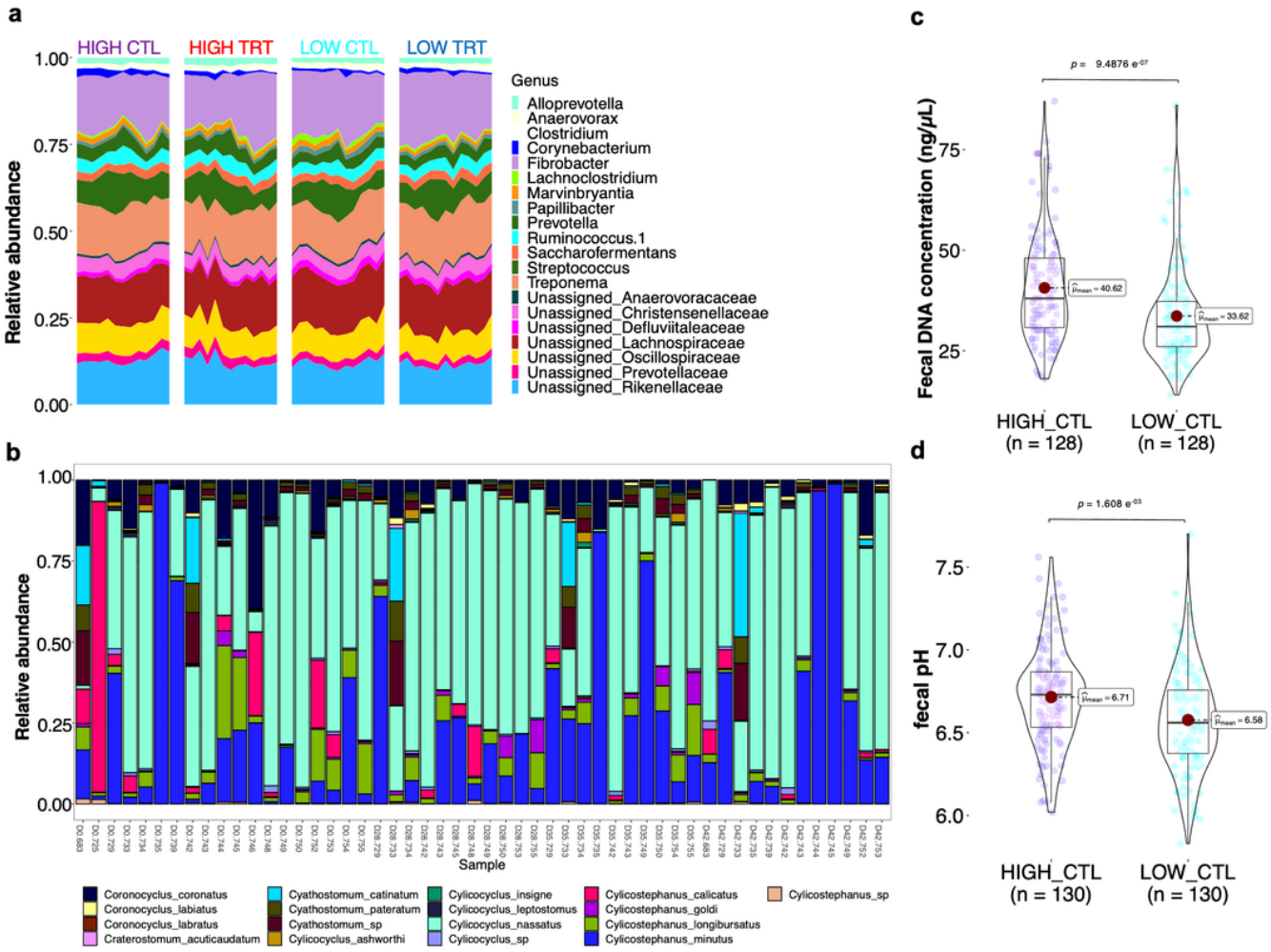

Figure 1

Global overview of the host - cyathostomin - gut microbiota system

(a) Taxonomic bar plots of the top 20 dominant genera in the gut microbiota according to the experimental groups. Colours denote microbial genera. Taxonomic inference relied on the QIIME closed-reference approach against the SILVA database at a sequence similarity level of 99%; (b) Relative abundances measured in the cyathostomin community in high shedders using ITS-2 barcodes; (c-d) Violin plots showing the concentration of faecal DNA and pH in faeces, respectively, according to the HIGH and LOW control groups. Boxplots show the median, 25th, and 75th percentile, the whiskers indicate the minima and maxima, and the points lying outside the whiskers of box plots represent the outliers. Adjusted p values from two-sided Wilcoxon rank-sum test

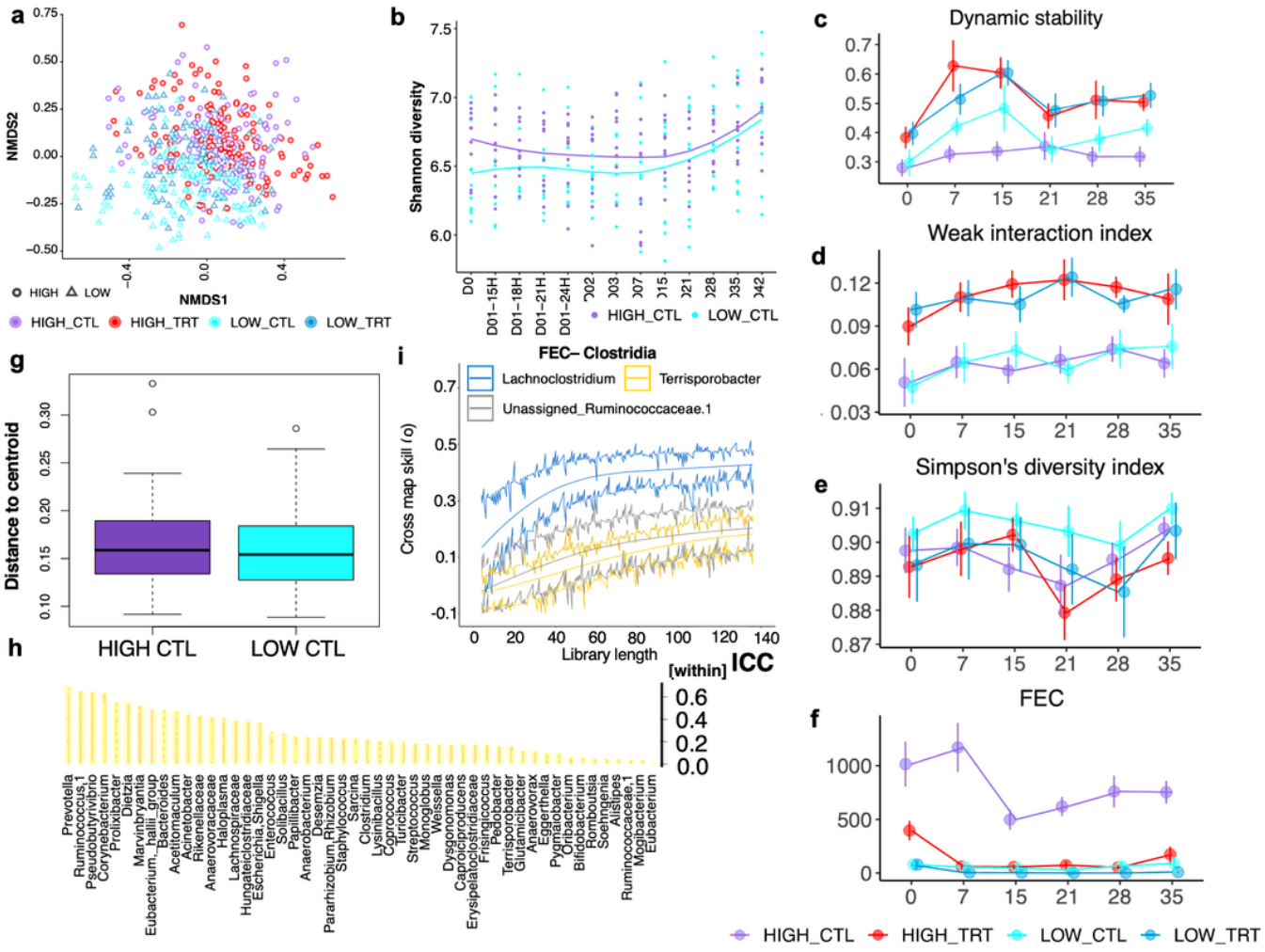

Figure 2

Helminth infection defines a stable assemblage despite the higher microbial richness and species turnover in infected ponies

(a) NMDS ordination analysis (Bray Curtis distance) of the ASV composition. Points denote individual samples which are coloured according to the experimental group: HIGH_CTL (violet), HIGH_TRT (red), LOW_CTL (cyan), and LOW_TRT (blue). The shape of the dots indicates the level of parasitism: round (HIGH) and triangle (LOW); (b) Longitudinal evolution of Shannon diversity across time for high and low shedding individuals. Shaded areas represent 95% confidence intervals; (c-f) Time-varying stability, interaction strength, Simpson's diversity index and FEC value for the microbial communities in each group using the Multispatial convergent cross-mapping; (g) Bray Curtis distance to the centroid of the gut microbial ASVs between the HIGH and LOW control groups. Boxes show median and interquartile range, and whiskers indicate 5th to 95th percentile; (h) Within-subject variance based on the interclass correlation coefficient (ICC) as part of the total variance in genus abundance for all genera significantly affected between high and low shedders across time; (i) Multispatial convergent cross-mapping (CCM) results showing causal relationships between FEC and the abundances of different taxa. Solid lines indicate

cross-map skill (ρ) from dynamic stability to another variable, which represents the causal influence of that variable on dynamic stability. Shaded regions indicate 95% confidence intervals of 1 000 surrogate time series. Cross-map skills (ρ) reported here were all significant

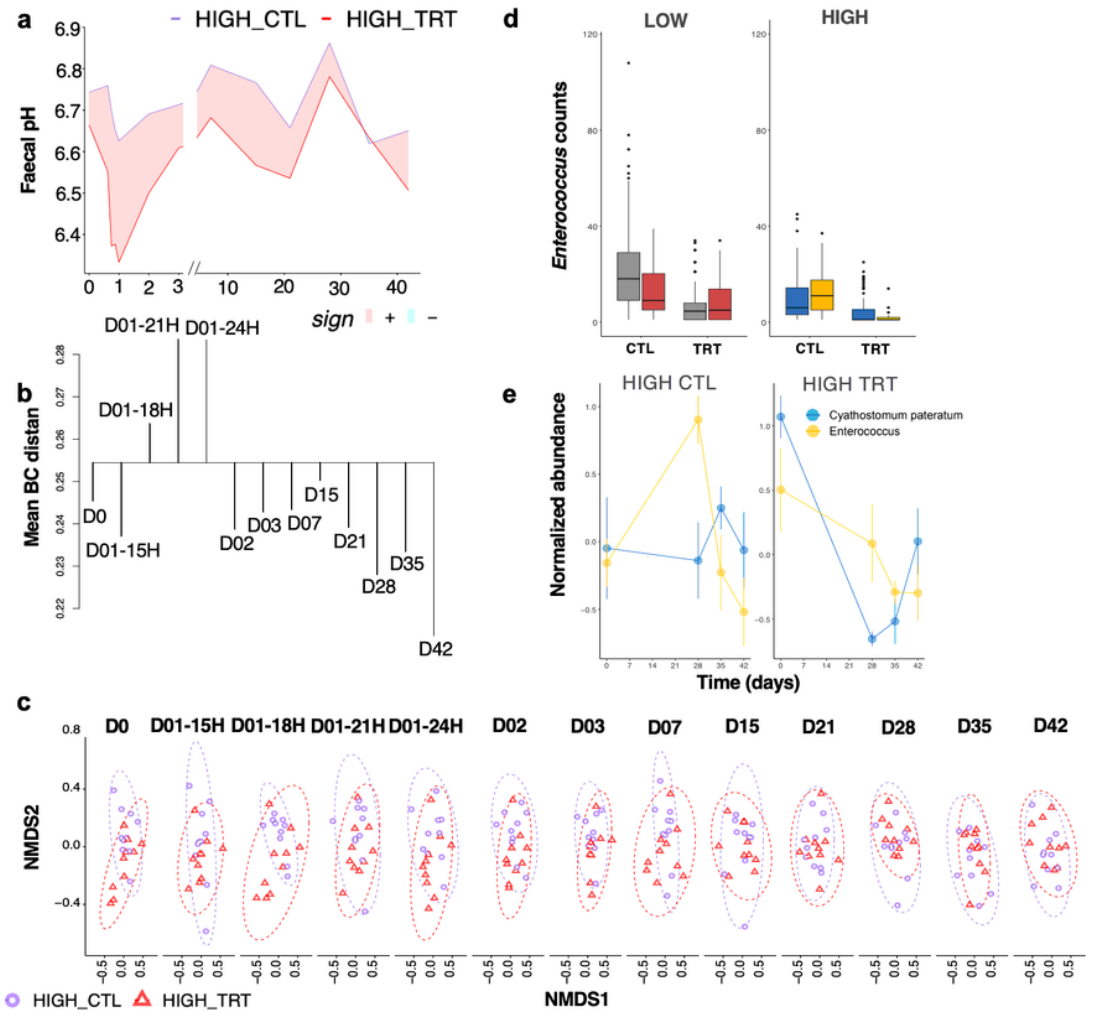

Figure 3

Parasite removal has a drastic effect on the gut environment and microbiota composition, but limited response in the host blood

(a) Evolution of faecal pH across time in high shedders. To display differences between group series, the ribbon was filled with red colour when the max in HIGH-CTL was higher than the min in HIGH-TRT, and in cyan colour when the maximum in HIGH-TRT was higher than the min in HIGH-CTL; (b) Dendrogram plot based on the within-time and between time dissimilarities in the HIGH-TRT group. The leaf segment is reversed if some time points are more heterogeneous than the combined time class. The horizontal line is drawn at the level of mean between-time dissimilarity, and vertical lines connect within-time dissimilarities to this line; (c) NMDS ordination analysis (Bray-Curtis distance) of the ASV composition in HIGH_CTL (violet), and HIGH_TRT (red) samples across the time points; (d) *Enterococcus* count distribution in the untreated (CTL) and treated (TRT) low- and high-shedders. Boxplots are coloured

according to whether counts were measured before (grey or blue) or after (red or yellow) significant parasite reappearance period (28 days after pyrantel treatment); (e) Trajectory of *Enterococcus* and *Cyathostomum pateratum* in the infected untreated and treated ponies

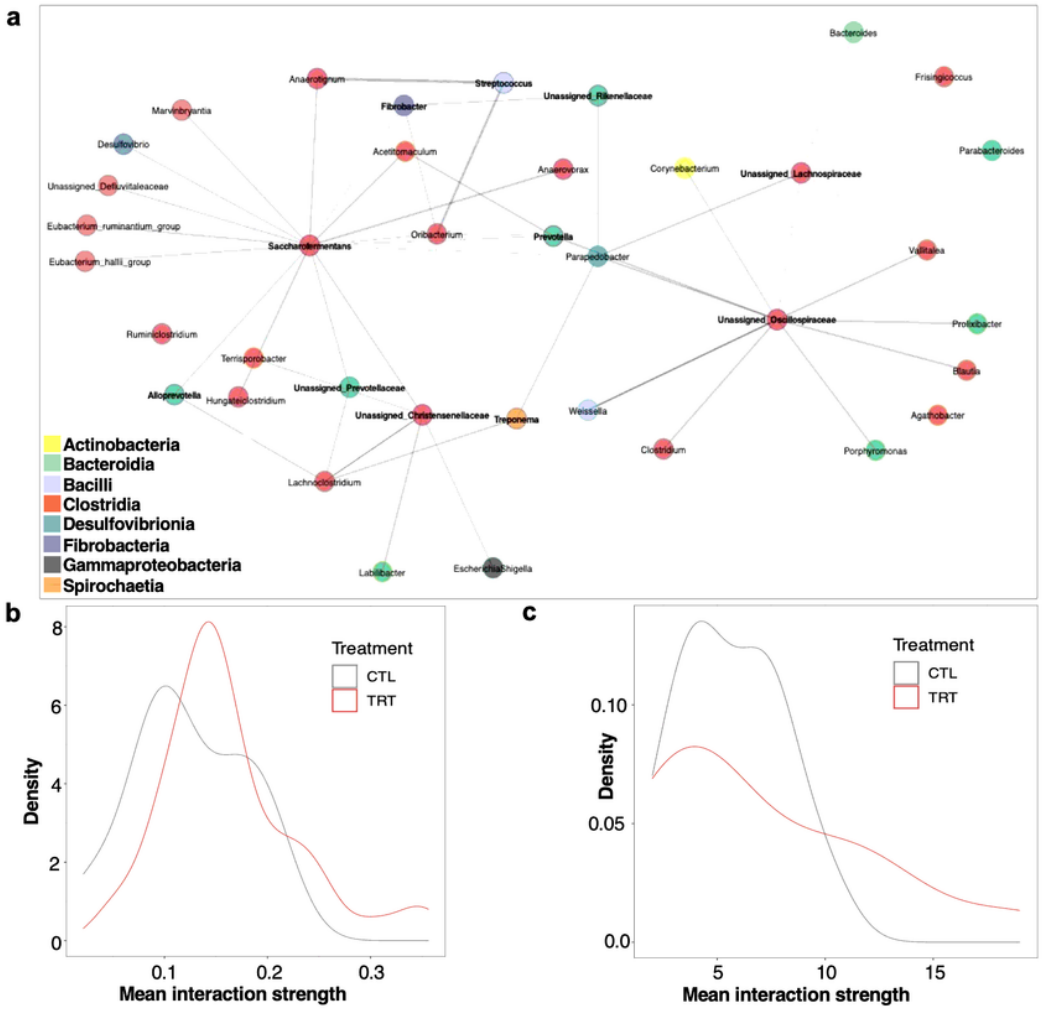

Figure 4

Core taxa connection ensures ecosystem stability upon environmental perturbations

(a) Ecological association inference of core taxa using the S-map method. Microbial nodes are coloured by order. Taxa highlighted in bold represents the core clades. Edge width corresponds to the strength of the association between features (S-map coefficients); (b-c) Density plot of all interactions and their strength in response to treatment

Supplementary Files

This is a list of supplementary files associated with this preprint. Click to download.

- SupplementaryInformation.pdf

- FigS1Cyathomix.tiff
- FigS2Cyathomix.tiff
- FigS3Cyathomix.tiff
- FigS4Cyathomix.tiff
- FigS5Cyathomix.tiff
- FigS6Cyathomix.tiff
- FigS7Cyathomix.tiff
- FigS8Cyathomix.tiff
- FigS9Cyathomix.tiff
- FigS10Cyathomix.tiff
- FigS11Cyathomix.tiff
- FigS12Cyahtomix.tiff
- FigS13Cyathomix.tiff
- FigS14Cyathomix.tiff
- FigS15Cyathomix.tiff
- FigS16Cyathomix.tiff
- FigS17Cyathomix.tiff
- FigS18Cyathomix.tiff
- FigS19Cyathomix.tiff
- SupplementaryTableS1Cyathomix.xlsx
- SupplementaryTableS2Cyathomix.xlsx
- SupplementaryTableS3Cyathomix.xlsx
- SupplementaryTableS4Cyathomix.xlsx
- SupplementaryTableS5Cyathomix.xlsx
- SupplementaryTableS6Cyathomix.xlsx
- SupplementaryTableS7CyathomixL.xlsx
- SupplementaryTableS8Cyathomix.xlsx
- SupplementaryTableS9Cyathomix.xlsx
- SupplementaryTableS10Cyathomix.xlsx
- SupplementaryTableS11Cyathomix.xlsx
- SupplementaryTableS12Cyathomix.xlsx
- SupplementaryTableS13Cyathomix.xlsx
- SupplementaryTableS14Cyathomix.xlsx
- SupplementaryTableS15Cyathomix.xlsx